Prefusion-specific glycoprotein B human antibodies protect against neonatal HSV-2 infection

Parastoo Amlashi[1,2]†, Jeongryeol Kim[3]†, Nisali N. Mendis[6,7], Perry T. Wasdin[1,2,4,5] Lindsay E. Bass[2], Gwen Jordaan[1,2], Alexandra A. Abu-Shmais[1,2], Matthew D. Slein[3], Nicole V. Johnson[3], Rachel H. Bonami[2,14,15,16], David A. Leib[6], Margaret E. Ackerman[6,7], Jason S. McLellan[3]*, Ivelin S. Georgiev[1,2,4,5,8,9,10,11,12,13]*

[1]Vanderbilt Center for Antibody Therapeutics, Vanderbilt University Medical Center, Nashville, TN 37232, USA

[2]Department of Pathology, Microbiology and Immunology, Vanderbilt University Medical Center, Nashville, TN 37232, USA

[3]Department of Molecular Biosciences, The University of Texas at Austin, Austin, TX 78712, USA

[4]Program in Chemical and Physical Biology, Vanderbilt University Medical Center, Nashville, TN 37232, USA

[5]Center for Computational Microbiology and Immunology, Vanderbilt University Medical Center, Nashville, TN 37232, USA

[6]Department of Microbiology and Immunology, Geisel School of Medicine at Dartmouth, Lebanon, NH 03756, USA

[7]Thayer School of Engineering, Dartmouth College, Hanover, NH 03755, USA

[8]Vanderbilt Institute for Infection, Immunology and Inflammation, Vanderbilt University Medical Center, Nashville, TN 37232, USA

[9]Department of Computer Science, Vanderbilt University, Nashville, TN 37232, USA

[10]Center for Structural Biology, Vanderbilt University, Nashville, TN 37232, USA

[11]Department of Biomedical Informatics, Vanderbilt University Medical Center, Nashville, TN 37232, USA

[12]Department of Chemical and Biomolecular Engineering, Vanderbilt University, Nashville, TN 37232, USA

[13]Department of Biochemistry, Vanderbilt University School of Medicine, Nashville, TN 37237, USA

[14]Division of Rheumatology and Immunology, Department of Medicine, Vanderbilt University Medical Center, Nashville, TN, USA

[15]Vanderbilt Center for Immunobiology, Vanderbilt University Medical Center, Nashville, TN 37232, USA

[16]Vanderbilt Institute for Infection, Immunology and Inflammation, Vanderbilt University Medical Center, Nashville, TN 37232, USA

†These authors contributed equally to this work

*Correspondence: jmclellan@austin.utexas.edu, ivelin.georgiev@vumc.org

ABSTRACT

Herpes simplex virus (HSV) can cause severe perinatal viral infections, leading to mortality or long-term neurological disability[1,2]. To date, antivirals have limited efficacy, and no vaccines are approved[3,4]. HSV entry requires the coordinated action of multiple viral glycoproteins. Glycoprotein B (gB), the most conserved glycoprotein among herpesviruses, mediates membrane fusion by undergoing a conformational transition from a metastable prefusion state to a stable postfusion state[5]. Potently neutralizing human antibodies targeting prefusion-specific epitopes have been identified for many virus families[6-10], however, such antibodies for human herpesviruses are currently limited to an alpaca-derived nanobody and a murine monoclonal antibody[11,12]. In this study, we used stabilized HSV-2 prefusion gB and LIBRA-seq single-cell sequencing technology[13] to probe B cells from HSV-2 seropositive and healthy human donors, resulting in the isolation of four prefusion-specific and two prefusion-preferring human antibodies. Cryo-EM studies revealed that the four prefusion-specific antibodies bind distinct epitopes on prefusion gB and exhibit different mechanisms of prefusion specificity. Two antibodies, 5-18 and 3-6, showed potent cross-neutralizing activity against HSV-1 and HSV-2 and conferred protection in a neonatal mouse model of HSV-2 infection. These findings highlight the molecular and structural determinants of HSV-2 prefusion gB recognition by human antibodies and demonstrate the translational potential of prefusion-specific gB antibodies.

INTRODUCTION

Herpes simplex viruses (HSV) are enveloped, double-stranded DNA alphaherpesviruses that establish lifelong infection in the peripheral nervous system and cause mucocutaneous disease[2]. HSV-1 typically presents as orolabial infection, whereas HSV-2 is associated with recurrent genital lesions and episodic viral shedding[14]. Globally, an estimated 13% of individuals aged 15–49 are infected with HSV-2, highlighting its persistent circulation and high seroprevalence[15]. Beyond mucocutaneous disease, HSV-2 contributes significantly to morbidity through neurologic complications and severe outcomes in neonates and immunocompromised individuals[16]. Neonatal HSV-2 infection, most commonly resulting from vertical transmission during birth, can cause long-term neurological impairment or death[17]. Current treatment relies on nucleoside analogs such as acyclovir, and although high-dose regimens improve survival in neonates, the risks of neurodevelopmental sequelae and relapse remain considerable[18,19]. Despite antiviral therapy, disseminated neonatal HSV-2 infection retains a mortality rate of approximately 30%[18,20], underscoring the urgent need for both preventive and adjunctive therapies. In this context, monoclonal antibodies (mAbs) targeting essential viral glycoproteins represent a promising avenue for therapeutic development.

HSV entry depends on a coordinated mechanism involving the surface glycoproteins gB, gD, and the gH/gL complex[21]. Entry is initiated by the receptor-binding gD, which activates the gH/gL heterodimer to trigger the membrane fusogen gB, a homotrimer that drives fusion of the viral and host cell membranes[22-24]. gB is highly conserved across herpesviruses and plays a critical role in viral attachment and fusion, making it an attractive target for the development of vaccines and antibodies[14,25]. As a class III fusion protein, gB undergoes a large-scale conformational rearrangement from a metastable prefusion state to a stable postfusion state[26,27]. Stabilizing gB in

42 its prefusion state provides a promising strategy for eliciting potent neutralizing antibody
43 responses, as the prefusion conformation presents unique antibody-accessible sites that are
44 concealed or disrupted in the postfusion conformation, as demonstrated for other viral fusion
45 proteins[28,29]. Indeed, antibodies targeting prefusion-specific epitopes on other viral fusion proteins
46 have been shown to exhibit potent neutralizing activity[6-10]. However, the structural transition of
47 gB primarily involves domain rearrangements rather than the secondary-structure refolding
48 characteristic of class I fusion proteins, and stabilizing the prefusion state has proven technically
49 challenging, hindering the isolation of prefusion-specific gB antibodies[12,30]. Although a camelid
50 nanobody[11] and a murine mAb[12], both elicited by immunization with recombinant antigens, were
51 recently shown to specifically recognize HSV prefusion gB, it remains unknown whether natural
52 human infection elicits similar prefusion-specific antibody responses and whether such antibodies
53 confer potent neutralization or protection from morbidity and mortality.

54 Although several mAbs protect against HSV-1/2 in preclinical models, most target gD;
55 only a few target gB, fewer still are human-derived, and none are prefusion-specific[31-36]. The gB
56 ectodomain consists of five structural domains, and most potently neutralizing gB-specific
57 antibodies recognize domains I, II, and IV[37-39] (**Supplemental Fig. 1**). Notably, HDIT101, a
58 humanized mAb targeting domain I, did not demonstrate superiority over standard-of-care therapy
59 in a phase 2 clinical trial for recurrent genital herpes[40,41]. These findings underscore the importance
60 of further delineating the antigenic landscape of prefusion gB and comprehensively profiling the
61 human B-cell response to HSV-2, both of which remain critical for informing next-generation
62 vaccine development and antibody-based interventions.

63 To address these knowledge gaps, we characterized the HSV-2 gB-specific B-cell
64 repertoire in HSV-2 seropositive individuals and healthy individuals with no recorded history of

65 HSV infection. Using the LIBRA-seq (Linking B cell Receptor Sequence to Antigen Specificity
66 through Sequencing) antibody-discovery technology[13], we identified four prefusion-specific and
67 two prefusion-preferring antibodies from human peripheral blood mononuclear cell (PBMC)
68 samples. Two prefusion-specific antibodies, 5-18 and 3-6, exhibited potent cross-neutralizing
69 activity against clinical isolates of both HSV-1 and HSV-2. To define the structural basis of their
70 specificity, we determined cryo-electron microscopy (cryo-EM) structures of a prefusion-
71 stabilized HSV-2 gB ectodomain in complex with the antigen-binding fragments (Fabs) of each
72 antibody. Fab 5-18, along with another prefusion-specific Fab 1-14, recognize quaternary epitopes
73 that span domains I and IV of adjacent protomers, whereas Fab 3-6 binds a distinct epitope that
74 bridges domains I and II and the intervening hinge region. Finally, both 5-18 and 3-6 conferred
75 protection in a well-established neonatal mouse model of HSV-2 infection, underscoring their
76 potential as candidate antibody-based interventions to prevent neonatal HSV-2 infection and
77 associated mortality.

78 **RESULTS**

79 **Identification of a diverse set of HSV-2 prefusion gB-specific mAbs by LIBRA-seq**

80 We applied LIBRA-seq to identify HSV-2 prefusion gB-specific B cells from human donor
81 PBMCs. The LIBRA-seq antigen panel included stabilized prefusion and postfusion gB constructs
82 from several clinically relevant human herpesviruses, including HSV-2, human cytomegalovirus
83 (HCMV), and Epstein-Barr virus (EBV), as well as control antigens HIV BG505 gp140 V9.3
84 SOSIP and influenza HA NC99, intended to filter out cells with non-specific binding activity.
85 Prefusion-stabilized gB constructs used were HSV-2 gB-G3[42], HCMV gB C7[43] (PDB ID: 7KDP),
86 EBV gB C3-GT[44] (PDB ID: 9OAL), as well as the postfusion gB ectodomain base constructs of
87 each herpesvirus. After LIBRA-seq sequencing and computational filtering as previously

88 described[13], we isolated a total of 449 antigen-specific B cells from eight donors: three with
89 confirmed HSV-2 seropositivity, three with confirmed HCMV seropositivity, and two healthy
90 donors with no recorded history of HSV or HCMV. A LIBRA-seq score (LSS) of 1 or greater was
91 selected as a cutoff to identify B cells predicted to have specificity for HSV-2 gB. A total of 69 B
92 cells had an LSS ≥1 for HSV-2 prefusion gB, and 75 had an LSS ≥1 for HSV-2 postfusion gB,
93 with some B cells having an LSS of ≥1 for both. Of these, we initially selected 22 clonally distinct
94 antibodies with diverse sequence characteristics and varying LIBRA-seq scores for HSV-2
95 prefusion gB and postfusion gB (**Fig. 1a**).

96 These 22 antibodies were produced recombinantly as IgG1 mAbs and screened for binding
97 by indirect enzyme-linked immunosorbent assay (ELISA). The selected antibodies bound either
98 prefusion gB, postfusion gB, or both (**Extended Data Fig. 1a**). To further explore the potential
99 for identifying prefusion-specific human antibodies against HSV-2 gB, we specifically focused on
100 six antibodies that showed: (1) high prefusion and low postfusion gB LIBRA-seq scores (**Fig. 1b**)
101 and/or (2) stronger antibody binding for prefusion than postfusion gB by ELISA (**Extended Data**
102 **Fig. 1b**). Biolayer interferometry (BLI) experiments were performed to assess the conformational
103 specificity of the isolated antibodies. In these experiments, the IgGs were immobilized to anti-
104 human IgG Fc Capture tips and assessed for binding to prefusion- and postfusion-stabilized HSV-
105 2 gB ectodomains at 200 nM, a concentration sufficient to observe high-affinity interactions.
106 Antibodies 5-18, 1-14, 3-6, and 3-5 each displayed saturated binding to prefusion-stabilized gB
107 but negligible binding to postfusion gB, indicative of prefusion-specific binding (**Fig. 1c**).
108 Antibodies 1-13 and 5-13 bound both proteins well, but with a faster on-rate for prefusion gB,
109 indicative of a preference for the prefusion conformation. Conversely, anti-HSV gB antibody
110 D48[45] bound both pre- and postfusion gB but had a faster on-rate for postfusion gB. Overall, four

111 antibodies were classified as prefusion-specific and two as prefusion-preferring based on their
112 reactivity to the two stabilized ectodomains, with the BLI data generally in agreement with
113 LIBRA-seq results.

114 To assess how common the HSV-2 gB prefusion-specific and prefusion-preferring
115 antibodies are in the general population, these mAb sequences were compared against a general
116 database of 1.7 million paired antibodies (**Extended Data Fig. 2a**). Several prefusion-specific
117 mAbs exhibited matches with ≥70% HCDR3 identity, most prominently mAb 3-5 (4,498 matches),
118 with fewer matches observed for 5-18 (20 matches) and 3-6 (2 matches), and none for 1-14
119 (**Extended Data Fig. 2b**). However, no prefusion-specific mAbs shared both heavy and light chain
120 V gene usage with antibodies in the database. Although mAb 5-18 showed multiple VH-matched
121 pairs with high HCDR3 identity, none met the criteria for full clones due to a lack of shared VL
122 usage. Among prefusion-preferring mAbs, 5-13 yielded 163 matches and included a single full
123 clone with matched VH and VL genes and ≥70% CDR3 identity, whereas mAb 1-14 showed no
124 such matches (**Extended Data Fig. 2b**). Together, these analyses suggest that no true public
125 clonotypes could be identified for the prefusion-specific gB mAbs from our study.

126 **Prefusion-specific gB antibodies potently neutralize HSV**

127 To investigate epitope groups on prefusion HSV-2 gB, we performed a pairwise
128 competition ELISA with all 22 antibodies initially identified from the dataset (**Fig. 2a**). The
129 patterns of binding-inhibition among antibody pairs compared to signal with no antibody
130 competition suggested the existence of at least one shared epitope on prefusion gB, as well as
131 clusters of antibodies that target overlapping or closely positioned binding regions (**Fig. 2b**). To
132 further characterize these interactions, we measured the binding affinities of the Fabs to prefusion-
133 stabilized HSV-2 gB via BLI (**Fig. 2c**, **Extended Data Fig. 3**). Both prefusion-specific and

134 prefusion-preferring mAbs exhibited picomolar affinities for prefusion-stabilized HSV-2 gB.
135 Among them, Fab 1-14 showed the strongest binding, with an equilibrium dissociation constant
136 (K_d) of 0.03 nM and a dissociation rate constant (k_{off}) at the instrument's limit of detection ($1.2 \times$
137 10^{-5} s^{-1}). Prefusion-specific Fab 3-6 exhibited a K_d of 0.12 nM and a k_{off} of 5.3×10^{-5} s^{-1}. Given
138 the high sequence similarity between HSV-2 and HSV-1 gB, we produced a prefusion-stabilized
139 HSV-1 gB ectodomain construct by applying the same stabilizing substitutions developed for
140 HSV-2 gB (**Extended Data Figs. 4**, **5a–c**). Binding affinities of the antibodies for the prefusion-
141 stabilized HSV-1 gB were then determined via BLI by immobilizing HSV-1 prefusion gB to Ni^{2+}-
142 NTA tips and dipping into Fab (**Fig. 2c**, **Extended Data Fig. 5d**). Fab 3-6 exhibited a slightly
143 improved affinity (K_d = 0.08 nM), driven by a faster association rate constant (k_{on} = 9.8×10^5
144 $M^{-1}s^{-1}$). In contrast, Fab 5-18 showed substantially reduced binding to HSV-1 gB, with a faster
145 dissociation rate constant and lower overall affinity (K_d = 40 nM). Fabs 1-14 and 3-5 bound HSV-
146 1 gB with affinities comparable to those observed for HSV-2 gB.

147 We next assessed the neutralization activity of the mAbs against the prototypic HSV-2
148 strain G via plaque-reduction assay (**Fig. 2d**). mAb 3-6 exhibited the most potent neutralization
149 (IC_{50} = 0.29 nM), exceeding well-characterized antibodies such as D48 (IC_{50} = 0.50 nM) and
150 HSV8 (an anti-gD antibody; IC_{50} = 0.51 nM). mAb 5-18 (IC_{50} = 1.25 nM) and 1-14 (IC_{50} = 1.44
151 nM) were also potent and showed comparable neutralizing activity (**Fig. 2e**). In contrast, 3-5 was
152 relatively weakly neutralizing despite having an affinity similar to the other prefusion-specific
153 antibodies. We also evaluated the neutralization activity of these prefusion-specific antibodies
154 against the clinical HSV-1 strain NS. Consistent with results for HSV-2, mAb 3-6 exhibited the
155 most potent neutralizing activity (IC_{50} = 0.34 nM), exceeding that of D48 (IC_{50} = 1.66 nM). mAb
156 5-18 (IC_{50} = 3.30 nM) was the next most potent, followed by 1-14 (IC_{50} = 33.46 nM). In contrast,

157 3-5 did not neutralize HSV-1 NS infection at the concentrations tested. These findings demonstrate
158 that HSV-2 prefusion-specific gB antibodies can cross-react with HSV-1 gB, and that 3-6 is the
159 most potent antibody against both HSV-1 and HSV-2.

160 We next evaluated *in vitro* autoreactivity of the four prefusion-specific gB antibodies to
161 self-antigens using immortalized human epithelial cell lines. We determined intracellular and
162 extracellular IgG binding to live, permeabilized HEp-2 and HEK293T cells by flow cytometry. At
163 25 μg mL^{-1}, none of the prefusion-specific gB antibodies displayed extracellular binding to either
164 cell line (**Extended Data Table 1**). Although mAbs 1-14 and 5-18 exhibited low levels of
165 intracellular binding compared to the positive control antibodies 4E10 and 2F5, no such reactivity
166 was observed for mAbs 3-5 and 3-6 (**Extended Data Fig. 6**).

167 **Antibodies 5-18 and 1-14 recognize quaternary epitopes spanning domains I and IV of**
168 **adjacent protomers**

169 We determined cryo-EM structures of prefusion-stabilized HSV-2 gB ectodomain in
170 complex with Fabs 5-18 and 1-14 at 2.9 Å and 3.2 Å resolution, respectively, to investigate the
171 molecular basis of their prefusion-specific epitopes (**Fig. 3**, **Extended Data Fig. 7, 8**). Both
172 antibodies recognize quaternary epitopes spanning domains I and IV of adjacent protomers, but
173 through distinct interaction modes. Fab 5-18 makes extensive contacts with both domains, burying
174 a total surface area of 1,440 $Å^2$, with 835 $Å^2$ on domain I and 605 $Å^2$ on domain IV (**Fig. 3a**, **b**,
175 **Extended Data Fig. 9a**). The antibody forms 14 hydrogen bonds and 4 salt bridges with domain
176 I and 10 hydrogen bonds with domain IV (**Extended Data Table 2**). All three complementarity-
177 determining regions of the heavy chain (HCDRs) engage domain I. HCDR1 and HCDR2 recognize
178 domain I, whereas HCDR3 spans domains I and IV (**Extended Data Fig. 9b**). Complementarity-
179 determining regions of the light chain (LCDRs) 1 and 3 primarily interact with domain I, whereas

180 LCDR2 interacts extensively with domain IV, establishing a continuous hydrogen-bond network
181 that stabilizes the interface (**Extended Data Fig. 9c).** This distribution of the epitope on to adjacent
182 protomers suggests that binding of 5-18, as well as 1-14, prevents protomer separation and locks
183 gB in the prefusion conformation, providing a mechanistic basis for neutralization. Mapping the
184 epitope of 5-18 on to the structure of postfusion gB (PDB ID: 8RH2) reveals that the epitope is
185 disrupted in the postfusion conformation due to the reorientation of domain I relative to domain
186 IV, resulting in contact residues on gB separated by approximately 100 Å (**Fig. 3c**). Additionally,
187 some of the epitope residues on domain I are buried by domain V of an adjacent protomer in the
188 postfusion conformation, collectively providing a structural basis for the prefusion specificity of
189 5-18.

190 Fab 1-14 has a smaller binding footprint than 5-18, burying a total surface area of 1,125
191 $Å^2$ (**Fig. 3d, e**, **Extended Data Fig. 9d**). Notably, interactions with domain IV differ substantially:
192 1-14 buries 244 $Å^2$ on domain IV versus 605 $Å^2$ for 5-18. The majority of the 1-14 contacts are
193 mediated by HCDR2 and HCDR3, which make extensive interactions with the long loop between
194 β14 and β15 in domain I (**Extended Data Fig. 9e**). LCDR1 and LCDR3 primarily contact domain
195 I, whereas LCDR2 and framework 3 (FR3) make limited contacts with domain IV (buried surface
196 area of 121 $Å^2$), including residues in the N-terminal α1 helix (**Extended Data Fig. 9f**). Similar to
197 5-18, the epitope of 1-14 becomes discontinuous and partially buried in the postfusion
198 conformation, providing the structural basis for its prefusion-specificity (**Fig. 3f**).

199 Interestingly, the epitopes of 5-18 and 1-14 closely resemble the epitope targeted by a
200 recently described prefusion-specific gB-directed camelid nanobody Nb1_gbHSV[11], which
201 recognizes a quaternary epitope spanning domains I, III, and IV (**Extended Data Fig. 10**). An
202 epitope comparison shows that the Nb1_gbHSV contacts many of the same residues as Fabs 5-18

203 and 1-14, but the nanobody reaches more deeply into the space between domains I and IV,
204 contacting domain III (**Extended Data Fig. 10e-f**). By contrast, Fabs 5-18 and 1-14 form more
205 extensive contacts across domains I and IV (**Extended Data Fig. 10a-d**). These structural studies
206 reveal multiple solutions by the human and camelid immune systems to recognize a similar
207 quaternary epitope on prefusion gB proteins.

208 **Antibodies 3-6 and 3-5 bind distinct epitopes located within a single protomer**

209 Next, we determined a cryo-EM structure of a ternary complex of prefusion-stabilized
210 HSV-2 gB bound to Fabs 3-6 and 3-5 at a resolution of 3.1 Å (**Fig. 4a, Extended Data Fig. 11**).
211 Fab 3-6 engages an extensive interdomain epitope encompassing domains I, II, and the hinge
212 region connecting them, burying a total surface area of 886 Å^2 (**Fig. 4b**, **Extended Data Fig. 12a**).
213 Binding is mediated primarily by the heavy chain (806 Å^2), with a much smaller contribution from
214 the light chain (80 Å^2), involving a total of 16 hydrogen bonds and 1 salt bridge (**Extended Data**
215 **Table 3**). The FR1 and HCDR1 of the heavy chain interact with the α4 helix of domain II. HCDR1,
216 HCDR2, and HCDR3 form multiple hydrogen bonds with the backbone of hinge residues 351–
217 358, establishing an extensive interaction network (**Extended Data Fig. 12b**). Additionally,
218 Trp100$_{HCDR3}$ is inserted into a hydrophobic pocket in domain I formed by Tyr152, Tyr279, Phe295,
219 and Val352, burying 134 Å^2 of surface area (**Fig 4b**, **Extended Data Fig. 12c**).

220 Superposition of domain I from a Fab 3-6-bound protomer onto domain I of the postfusion
221 gB structure shows that domain II reorients in the postfusion conformation and would clash with
222 Fab 3-6 (**Fig. 4c**). The flexible hinge residues at the center of the epitope also undergo a
223 conformation change, distorting the epitope. Collectively, these rearrangements provide a
224 structural basis for the inability of 3-6 to bind trimeric postfusion gB. A recently reported prefusion
225 gB-specific murine mAb named WS.HSV-1.24[12] was shown to recognize a highly similar epitope,

226 but it is rotated about the heavy chain such that the light chain is on the opposite side relative to
227 that of 3-6 (**Extended Data Fig. 13a–d**). Overall, 3-6 targets a highly neutralization-sensitive
228 prefusion-specific epitope encompassing the hinge region between domains I and II, establishing
229 this site as a vulnerable region on HSV-2 gB.

230 Antibody 3-5 binds to an epitope at the tip of domain I, a region not previously known to
231 be targeted by gB-directed antibodies (**Fig. 4a**). This interaction enabled modeling of the domain
232 I residues near the fusion loops, which were disordered in the HSV-2 gB structures complexed
233 with 5-18 or 1-14. Fab 3-5 forms a large interface on domain I, burying a total of 1,296 $Å^2$ of
234 surface area. The heavy chain buries 980 $Å^2$, whereas the light chain buries only 316 $Å^2$. All heavy
235 chain CDRs, as well as FR1 and FR3, participate in the interaction with domain I, forming 16
236 hydrogen bonds (**Extended Data Table 3**). Residues in LCDR1 and LCDR3 form 7 hydrogen
237 bonds with residues in domain I, further extending the interaction surface (**Extended Data Table**
238 **3**). Interestingly, the angle of approach of Fab 3-5 is oriented upward from the membrane-proximal
239 side, likely preventing binding to the native, membrane-embedded prefusion gB trimer on virions.
240 Furthermore, the epitope overlaps with the membrane proximal region (MPR) helices that
241 sequester the fusion loop residues at the tip of domain I in the full-length prefusion conformation
242 (**Fig. 4d**). This limited epitope accessibility on the native virion could explain the poor neutralizing
243 activity of Fab 3-5 despite its high binding affinity for the prefusion-stabilized gB ectodomain
244 construct. The prefusion specificity of Fab 3-5 is explained by the steric clashes between its heavy
245 chain and domain I of the adjacent protomer in the postfusion conformation (**Fig. 4e**). Given that
246 3-5 is unable to bind postfusion gB trimers and is unlikely to bind prefusion membrane-anchored
247 trimers, this antibody may have been elicited against an intermediate conformation of gB.

248 **Conservation and glycan shielding of HSV-2 prefusion-specific epitopes across human**
249 **herpesvirus gBs**

250 We analyzed the sequence similarity and glycan shielding of the prefusion-specific
251 epitopes on HSV-2 gB targeted by mAbs 5-18 and 3-6 and compared these features across human
252 herpesvirus gBs, focusing on the betaherpesvirus HCMV and the gammaherpesvirus EBV
253 (**Extended Data Fig. 14**). Sequence conservation analysis revealed that the quaternary epitope
254 recognized by 5-18 is highly divergent among these viruses, with only 6 out of 44 contact residues
255 conserved in HCMV and 7 out of 44 in EBV (**Extended Data Fig. 14a**). The epitope targeted by
256 3-6 also shows low conservation across these viruses, with 4 out of 24 residues conserved in
257 HCMV and 8 out of 24 in EBV. Notably, the hinge region within this epitope is highly variable
258 among human herpesvirus gBs, reflecting the divergent evolution of this site (**Extended Data Fig.**
259 **14b**). It is therefore unlikely that broadly reactive, pan-herpesvirus antibodies will be elicited
260 against either site on gB.

261 In addition to sequence conservation, we also analyzed the glycan shielding of these
262 epitopes. HSV-2 gB contains six N-linked glycosylation sites per protomer, four of which are
263 resolved in our structures. Domains I and IV, which are major targets of neutralizing antibodies,
264 lack glycosylation, and the quaternary epitopes recognized by 5-18 and 1-14 remain unshielded in
265 HSV-2 gB (**Extended Data Fig. 14c**). An N-linked glycan at Asn671 is positioned near Fab 3-6,
266 but this does not prevent the antibody from binding (**Extended Data Fig. 14c**). We next examined
267 glycan shielding of prefusion epitopes on HCMV[46] and EBV[47] gB, for which glycans were
268 modeled using Glycoshape[48] (**Extended Data Fig. 14c**). Structural analysis of the 5-18 contact
269 sites on HCMV and EBV gB shows that, although the glycans at Asn586 and Asn555 in HCMV
270 and Asn563 in EBV are positioned at the edge of the contact interface in domain IV, the major

271 contact surfaces of the 5-18 epitope remain largely unshielded in both viruses (**Extended Data**
272 **Fig. 14c**). In contrast, the 3-6 binding site, particularly the hinge region, contains a glycan in both
273 HCMV (Asn341) and EBV (Asn290), suggesting glycan-mediated masking of a site that is highly
274 vulnerable on HSV-2 gB (**Extended Data Fig. 14c**). Notably, this hinge-region glycan is
275 conserved in HCMV, EBV, and HHV-6, but is absent from HSV-1, VZV, KSHV, and HHV-7,
276 indicating divergent glycan-shielding strategies among human herpesviruses (**Extended Data Fig.**
277 **14b**).

278 **Prefusion-specific gB antibodies protect from HSV-2 challenge in a neonatal mouse model**

279 Given the strong neutralizing activity of 3-6, 5-18, and 1-14, we assessed their ability to
280 protect mice from a lethal challenge of HSV2-CNS11, a highly virulent clinical isolate. Briefly, 2-
281 day-old C57BL/6J pups were administered 80 μg of mAb intraperitoneally (i.p), followed by an
282 immediate intranasal (i.n.) challenge with 500 plaque-forming units (PFU) of HSV2-CNS11 (**Fig.**
283 **5**). Each of the three tested prefusion gB-specific mAbs provided statistically significant ($p \leq 0.002$)
284 partial protection at this treatment dose, as compared to the VRC01 control. All animals treated
285 with the negative control HIV-1 envelope-directed mAb VRC01 failed to survive infection. At day
286 21 post-infection, the protection afforded by 3-6 was equivalent to that provided by HSV8 (gD-
287 specific), with an overall survival rate of 91%. Treatment with 5-18 afforded 75% protection,
288 which was comparable to but lower than the 87% protection provided by the gB-specific control
289 mAb D48. Antibody 1-14 provided the least protection (20%). Collectively, these data demonstrate
290 that mAb 3-6 can confer a high degree of protection against a lethal HSV2-CNS11 challenge in a
291 neonatal mouse model, equivalent to that afforded by the gD-directed mAb HSV8.

292 **DISCUSSION**

293 HSV is a widespread and clinically significant human pathogen that disproportionately
294 affects vulnerable populations. Notably, HSV is an etiologic agent of neurologic and neonatal
295 disease, often resulting in lifelong complications and substantial direct and indirect healthcare
296 costs[49,50]. Preclinical studies have demonstrated that protective mAbs are highly effective for
297 controlling perinatal HSV infection[31,33,40,41]; however, the structural and molecular basis of
298 antibody recognition of the viral fusion glycoprotein B (gB)—particularly in its prefusion
299 conformation—remains poorly defined. Here, we describe the identification of human antibodies
300 that recognize epitopes exclusive to prefusion gB and potently cross-neutralize both HSV-1 and
301 HSV-2. Two such antibodies, 5-18 and 3-6, conferred strong protection against lethal HSV-2
302 infection in a neonatal mouse model, further underscoring their therapeutic potential.

303 Prior to this work, prefusion-specific human antibodies targeting gB had not been
304 characterized. This likely reflects both the substantial similarity between the exposed surfaces on
305 prefusion and postfusion gB and the lack of prefusion-stabilized gB probes for B-cell sorting.
306 Recently, a prefusion-specific camelid nanobody and a prefusion-specific murine antibody were
307 isolated following immunization with vesicle-displayed native HSV-1 gB[11] or prefusion-stabilized
308 HSV-1 gB[12], respectively; however, large-scale screening of human B cells specifically targeting
309 prefusion gB has not been reported. Here, we address this limitation by applying LIBRA-seq with
310 a prefusion-stabilized HSV-2 gB antigen[42] to PBMCs from HSV-seropositive donors, enabling the
311 isolation of human prefusion-specific antibodies and the identification of previously
312 uncharacterized vulnerable epitopes on HSV gB. With the recent development of soluble,
313 prefusion-stabilized herpesvirus gB antigens and high-resolution structural information[42-44], there
314 is now considerable potential to discover and develop additional potent prefusion gB-specific
315 antibodies. Although prefusion-specific antibodies targeting HCMV and EBV gB may differ from

316 those recognizing HSV-1 and HSV-2 gB due to distinct glycan shielding patterns (**Extended Data**
317 **Fig. 14c**), it will be important to determine whether similarly potent neutralizing antibodies and
318 discrete prefusion-specific epitopes exist across herpesvirus gB orthologs.

319 Antibodies 5-18 and 3-6 potently neutralized both HSV-1 and HSV-2, with 3-6
320 demonstrating the greatest potency against both clinical isolates (**Fig. 2d**, **e**). When co-
321 administered with a lethal dose of HSV2-CNS11 in a neonatal mouse study, mAb 3-6 conferred
322 protection comparable to previously characterized neutralizing antibodies HSV8 (gD-specific) and
323 D48 (gB-specific), highlighting its therapeutic potential (**Fig. 5**). Given the multistep nature of
324 herpesvirus entry[51], therapeutic strategies employing antibody cocktails that target multiple
325 epitopes within a single glycoprotein or span distinct viral glycoproteins may provide enhanced
326 protection. Because gD mediates viral attachment[52] and gD-directed antibodies have been
327 extensively studied and have shown robust neutralizing activity[32], combining gD-specific
328 antibodies with prefusion gB-specific antibodies may represent an improved strategy for HSV
329 prevention or treatment. Such combinations would target sequential steps in viral entry and may
330 yield synergistic antiviral effects.

331 In these studies, we determined that the prefusion-specific antibody 3-5 binds a membrane-
332 proximal epitope on gB. Structural analysis indicates that 3-5 is unlikely to engage prefusion gB
333 in the viral membrane, as its predicted angle of approach would result in steric clashes with the
334 lipid bilayer and MPR helices. Consistent with this interpretation, 3-5 exhibits poor neutralizing
335 activity against HSV-2, suggesting that it may recognize an intermediate conformational state of
336 gB, such as after domain I has disengaged from the MPR but before insertion of the hydrophobic
337 fusion loops into the target cell membrane. Intermediate conformations of class III fusion proteins
338 have been visualized by cryo-electron tomography, including for vesicular stomatitis virus G[53].

339 Analogously, non-neutralizing prefusion-specific antibodies have been described for HIV-1,
340 where antibodies targeting membrane-proximal gp41 base epitopes are preferentially elicited,
341 thereby constraining the induction of broadly neutralizing responses[54,55]. Recent studies further
342 indicate that prefusion-stabilized HSV-2 gB elicits immune responses comparable to those induced
343 by postfusion gB[42], underscoring the challenge of selectively focusing humoral immunity on
344 functionally vulnerable prefusion epitopes. Systematic characterization of B cell lineages, coupled
345 with antigen-design strategies such as glycan shielding or epitope masking, can be utilized to
346 preferentially enhance the activation of B cells encoding potently neutralizing and protective
347 antibodies against HSV. Furthermore, the results from these studies suggest that potently
348 neutralizing mAbs targeting the prefusion form of gB represent an attractive therapeutic option for
349 preventing HSV-associated disease in vulnerable populations.

350 **ACKNOWLEDGMENTS**

351 We thank all members of the Georgiev laboratory and McLellan laboratory for their support and
352 feedback. We thank David Flaherty, Olivia Murfield, Emma McLaughlin, and Brittany Matlock
353 from the VUMC Flow Cytometry Shared Resource for their help with cell sorting. The VUMC
354 Flow Cytometry Shared Resource is supported by the Vanderbilt Ingram Cancer Center (P30
355 CA68485) and the Vanderbilt Digestive Disease Research Center (DK058404). We thank Angela
356 Jones, Jamie Roberson, and Latha Raju with the Vanderbilt Technologies for Advanced Genomics
357 Core (VANTAGE) for providing technical assistance with library production and sequencing.
358 VANTAGE is supported in part by CTSA (5UL1 RR024975-03), the Vanderbilt-Ingram Cancer
359 Center (P30 CA68485), the Vanderbilt Vision Center (P30 EY08126), and NIH/NCRR (G20
360 RR030956). We thank Dr. Axel Brilot and Dr. Evan Schwartz at the Sauer Structural Biology
361 Laboratory at UT Austin for assistance with cryo-EM data collection, which is supported in part

362 by The University of Texas at Austin College of Natural Sciences and award RR160023 of the
363 Cancer Prevention and Research Institute of Texas. For work described in this manuscript, I.S.G.,
364 P.A., G.J., P.T.W., and A.A.A. were supported in part by NIH R01AI175245, and J.S.M. was
365 supported in part by Welch Foundation grant number F-0003-19620604. L.E.B was supported by
366 NIH F31DK141224. N.N.M., D.A.L., and M.E.A. were supported by NIH R01AI176646. R.H.B.
367 was supported in part by NIH R01DK131070. The funders had no role in the conceptualization or
368 execution of any studies or drafting of the manuscript.

369 **AUTHOR CONTRIBUTIONS**

370 P.A., J.K., N.V.J., A.A.A., J.S.M., and I.S.G. conceived, designed, and directed the study. P.A.
371 and G.J. conducted the LIBRA-seq experiments. P.T.W. conducted the bioinformatic analysis.
372 P.A., J.K., N.N.M., L.E.B., and G.J. performed experiments. J.K. and N.V.J. designed protein
373 constructs and assisted with protein production. J.K. performed the structural and biophysical
374 studies. N.N.M., D.A.L., and M.E.A. led the functional studies. P.A., J.K., J.S.M., and I.S.G. wrote
375 the manuscript with input and feedback from all authors.

376 **DECLARATION OF INTERESTS**

377 P.A., J.K., N.N.M., D.A.L., M.E.A., J.S.M., and I.S.G. are listed as inventors on patents filed
378 describing the antibodies discovered here. I.S.G. is listed as an inventor on patent applications for
379 the LIBRA-seq technology. J.S.M. is listed as an inventor on a patent application describing
380 prefusion-stabilized HSV-2 gB proteins. I.S.G. is a co-founder of AbSeek Bio. I.S.G. has served
381 as a consultant for Sanofi. The Georgiev laboratory at VUMC has received unrelated funding from
382 Merck and Takeda Pharmaceuticals. The Ackerman laboratory at Dartmouth has received
383 unrelated funding from Be Bio and Moderna.

384

385 **METHODS**

386 **Cells and viruses**

387 FreeStyle 293F cells (Gibco), Expi293 cells (Gibco), Vero cells (ATCC, cat. no. CCL-81), HEp-
388 2 cells (ATCC, cat. no. CCL-23), and HEK293T cells (ATCC, cat. no. CRL-3216) were cultured
389 according to vendor instructions. Virus strains used in this study included HSV2-G [56], HSV1-NS[57],
390 and HSV2-CNS11[58]. For virus propagation, Vero cells were used to prepare viral stocks as
391 described previously[59,60].

392 **Mice**

393 C57BL/6J (RRID:IMSR_JAX:000664) mice were either purchased from The Jackson
394 Laboratories or bred in animal facilities at Dartmouth College in accordance with Institutional
395 Animal Care and Use Committee protocols (Dartmouth College IACUC protocol 2151).

396 **Human blood sample collection and preparation**

397 Prospective blood collection and peripheral blood mononuclear cell (PBMC) isolation from HSV-
398 2 positive donors were procured from BioCollections Worldwide, Inc. (Miami, FL) and certified
399 by BioPlex 2200 HSV-1 & HSV-2 IgG kit on the BioPlex 2200 System. Healthy donor PBMCs
400 with no recorded history of prior infection were purchased commercially from StemCell
401 Technologies (catalog number 70025.3). Samples arrived frozen and were stored at -135 °C until
402 use.

403 **HSV gB expression and purification**

404 HSV-1 gB ectodomain (Strain KOS; Uniprot: P06437, residues 31–725) was engineered in both
405 postfusion and prefusion-stabilized forms using the same prefusion-stabilizing substitutions as the
406 HSV-2 gB constructs (Strain HG52; Uniprot: P06763, residues 23–731; postfusion gB-B1 and

407 prefusion-stabilized gB-O3)[61]. For HSV-1 prefusion gB, the N-terminal disordered region
408 (residues 32–78) was truncated to improve expression, an interprotomer disulfide bond
409 (T243C/E679C) and two proline substitutions (S688P and T669P) were introduced to stabilize the
410 prefusion conformation, and substitutions H172N and Y174T were incorporated to reduce
411 aggregation (**Extended Data Fig.4**). All constructs were transiently expressed in FreeStyle 293F
412 cells using polyethylenimine (PEI) transfection reagent. Cultures were maintained at 37 °C and 8%
413 CO_2, and the media were harvested 6 days post-transfection. The supernatants were filtered
414 through a 0.22 µm membrane and loaded onto Strep-Tactin 4Flow resin (IBA Lifesciences) by
415 gravity. After washing with 100 mM Tris-HCl pH 8.0, 150 mM NaCl, and 1 mM EDTA, the bound
416 proteins were eluted with 100 mM Tris-HCl pH 8.0, 150 mM NaCl, 1 mM EDTA, and 50 mM
417 biotin (IBA Lifescience). The elution fractions were incubated overnight at 4 °C with 5% (w/w)
418 His-tagged HRV3C protease to remove purification tags. The samples were then purified by size-
419 exclusion chromatography (SEC) using a Superose 6 Increase 10/300 GL column (Cytiva)
420 equilibrated in phosphate-buffered saline (PBS).

421 **Oligonucleotide barcodes**

422 Oligonucleotides composed of a 15 bp antigen barcode were used with sequence modifications to
423 anneal to the template switch oligo on the 10x bead-delivered oligos and truncated TruSeq small
424 RNA read 1 sequence in the following structure: 5′
425 CCTTGGCACCCGAGAATTCCANNNNNNNNNNNNNCCCATATAAGA∗A∗A-3′, where N
426 represent the antigen barcode. For each antigen, we used the following barcode sequences: HSV-
427 2 gB-G3 prefusion (GACAAGTGATCTGCA), HSV-2 gB B1 postfusion
428 (AACCCACCGTTGTTA), HCMV gB C7 prefusion (CAGTAGATGGAGCAT), HCMV gB base
429 postfusion (ATCGTCGAGAGCTAG), EBV gB C3-GT prefusion (TGTGTATTCCCTTGT),

430 EBV gB base postfusion (GCTCCTTTACACGTA), HIV BG505 gp140 V9.3 SOSIP
431 (TCACAGTTCCTTGGA), and influenza HA NC99 (GGTAGCCCTAGAGTA). Oligos were
432 ordered from Sigma-Aldrich and IDT with a 5′ amino modification and HPLC purified.

433 **Antigen labeling with DNA oligonucleotide barcodes**

434 For each antigen, the unique DNA barcodes were directly conjugated using SoluLINK Protein-
435 Oligonucleotide Conjugation kit (Vector Labs, S-9011) according to the kit's protocol. Each
436 antigen was biotinylated using EZ link (Thermo), desalted and modified with S-HyNic. The 4FB-
437 modified DNA barcodes were directly conjugated to the biotinylated antigen with S-HyNic to
438 create a stable bond between the protein and oligonucleotide. The antigen-oligonucleotide
439 conjugate concentrations were determined using a bicinchoninic acid (BCA) assay, and the HyNic
440 molar substitution ratios of each antigen-oligonucleotide conjugate were determined using a
441 NanoDrop according to the SoluLINK protocol instructions. Excess oligonucleotides were
442 removed from the protein-oligonucleotide conjugates using an AKTA FPLC and were
443 subsequently verified using SDS-PAGE and silver stain. The optimal amounts of antigen-
444 oligonucleotide conjugates to be used in antigen-specific B cell sorting were then determined
445 through flow cytometry titration experiments on cell lines expressing BCRs of known specificities.

446 **Antigen-specific B cell sorting**

447 PBMCs were thawed and counted using Trypan Blue viability stain. Cells were washed with a
448 solution of Dulbecco's phosphate-buffered saline (DPBS) supplemented with 0.1% bovine serum
449 albumin (BSA). Samples were resuspended in DPBS-BSA and stained with cell markers: CD14
450 (BD, cat no. 301819, clone M5E2, 1:10), Ghost Dye Red 780 Viability (Cell Signaling Technology,
451 cat no. 18452S, 1:1000), CD3 (Cytek Biosciences, cat no. 35-0037, clone OKT3), CD19 (BD, cat
452 no. 563036, clone SJ25C1), and IgG (BD, cat no. 551497, clone G18 145). Samples were

453 resuspended in DPBS-BSA before surface staining for 30 min. Additionally, antigen-
454 oligonucleotide conjugates were incorporated into the stain. After 30 min incubation in the dark at
455 room temperature, cells were washed three times with DPBS-BSA at 300g for 5 min. Next, the
456 samples were incubated for 15 min at room temperature with Streptavidin-PE (Invitrogen, cat no.
457 S866) to label cells with bound antigen. The cells were again washed three times with DPBS-BSA,
458 resuspended in DPBS, and sorted by FACS. Antigen-positive B cells were bulk sorted and
459 sequenced at Vanderbilt Technologies for Advanced Genomics (VANTAGE) at an appropriate
460 target concentration for 10X Genomics library preparation and subsequent sequencing. FACS data
461 were analyzed using FlowJo (BD Biosciences).

462 **Sample and library preparation for sequencing**

463 Single-cell suspensions were processed using the Chromium Controller microfluidics device (10X
464 Genomics) and B cell Single Cells V(D)J solution as per the manufacturer's instructions. The aim
465 was to capture 10,000 B cells per 1/8 10X cassette. Slight modifications were made to intercept,
466 amplify, and purify the antigen barcode libraries, as previously described[62].

467 **Sequence processing and bioinformatics analysis**

468 For bioinformatic processing of the LIBRA-seq sequencing reads, we followed our established
469 pipeline, which takes paired-end FASTQ files of oligonucleotide libraries as input. This pipeline
470 processes and annotates reads for cell barcodes, unique molecular identifiers (UMIs) and antigen
471 barcodes, resulting in a cell-barcode and antigen-barcode UMI count matrix[13]. B cell receptor
472 contigs and antigen-barcode libraries were processed using CellRanger 3.1.0 (10x Genomics) with
473 GRCh38 Human V(D)J 7.0.0 as reference. From the BCR sequencing, 8,467 functional paired
474 heavy- and light-chain sequences were recovered. B cell receptor contigs were aligned to IMGT
475 reference genes using High-V Quest[63].

476 **Antibody expression and purification**

477 Variable heavy and light genes were inserted into custom plasmids that encode the constant region
478 for the human IgG1 heavy chain and respective lambda and kappa light chains (Genscript). The
479 antibodies were expressed in Expi293 cells by co-transfecting heavy chain and light chain
480 expression plasmids using PEI or Expifectamine transfection reagent (Thermo Fisher Scientific)
481 and cultured for 4–5 days. Cultures were harvested and centrifuged, and supernatant was filtered
482 through 0.45 μm Nalgene Rapid Flow Disposable Filter Units with PES membrane. The filtered
483 supernatant was run over a column containing Protein A agarose resin that was equilibrated with
484 PBS. The column was washed with PBS, and then the antibodies were eluted with 100 mM
485 glycine-HCl at pH 2.7 directly into a 1:10 volume of 1 M Tris-HCl pH 8.0. Eluted antibodies were
486 buffer exchanged into PBS using Amicon Ultra centrifugal filter units, centrifuging and topping
487 off three times with PBS, and finally concentrated. The antibodies were analyzed by SDS-PAGE.
488 Antibody plasmids were sequenced to confirm the expected heavy and light chains.

489 **Indirect enzyme-linked immunosorbent assay (ELISA)**

490 For indirect ELISA assays, maxisorp 96-well flat-bottomed plates (Thermo Fisher Scientific) were
491 coated with recombinant gB antigen at 2 μg mL^{-1} in PBS overnight at 4 °C. Subsequent washes
492 were performed with PBS-T (PBS supplemented with 0.05% v:v Tween20 (Millipore-Sigma)).
493 Blocking was performed in 5% BSA in PBS-T for 2 h at room temperature and then washed three
494 times with PBS-T. Primary antibodies were serially diluted 1:5 in 1% BSA in PBS-T with a starting
495 concentration of 10 μg mL^{-1} and incubated at room temperature for 1 h, washed, and detected via
496 a horseradish peroxidase-conjugated anti-mouse IgG secondary diluted 1:10,000 (Jackson
497 ImmunoResearch). One-step TMB-ELISA substrate solution (Thermo Fisher Scientific) was

498 added to develop for 5 min and quenched with 1 N sulfuric acid. Absorbance at 450 nm (A_{450}) was
499 measured on a microplate reader. ELISAs were performed in technical and biological duplicates.

500 **Antibody competition ELISA**

501 For competition ELISA assays, maxisorp 384-well microtiter plates (Thermo Fisher Scientific)
502 were coated with recombinant gB antigen at 2 μg mL^{-1} in PBS overnight at 4 °C. Subsequent
503 washes were performed three times with PBS-T. Blocking was performed in 5% BSA in PBS-T
504 for 2 h at room temperature, followed by three washes with PBS-T. Primary competitor antibodies
505 at 10 μg mL^{-1} were added to wells incubated for 1 h at room temperature. Without washing off the
506 competitor antibody, a biotinylated preparation of antibodies was added to wells with primary
507 antibody at a concentration of 1 μg mL^{-1} and incubated for 1 h at room temperature. Plates were
508 washed three times with PBS-T and bound antibodies were detected via a horseradish peroxidase-
509 conjugated mouse anti-biotin secondary diluted 1:4,000 (SouthernBiotech). One-step TMB-
510 ELISA substrate solution (Thermo Fisher Scientific) was added, incubated for 5 min, and
511 quenched with 1 N sulfuric acid. Absorbance at 450 nm (A_{450}) was measured on a microplate
512 reader. The A_{450} signal obtained for binding of the biotin-labelled reference antibody in the
513 presence of the unlabeled tested antibody was expressed as a percentage of the binding of the
514 reference antibody alone. Competition ELISAs were performed in technical and biological
515 duplicates.

516 **Prefusion specificity measurement**

517 Bio-layer interferometry (BLI) experiments were conducted on an OctetRED96e instrument
518 (Sartorius) at 21 °C with a shaking speed of 1000 rpm. For determination of prefusion specificity,
519 HSV-2 gB-specific IgG antibodies were immobilized onto anti-human IgG Fc Capture (AHC)
520 biosensors (Sartorius) to a response level of approximately 1.0 nm in HBS-EP buffer (10 mM

521 HEPES pH 7.4, 150 mM NaCl, 3 mM EDTA, 0.05% v/v surfactant P20) supplemented with 0.1 %
522 w/v BSA. Loaded sensors were then dipped into wells containing 200 nM of HSV-2 or HSV-1
523 prefusion-stabilized gB or postfusion gB for 180 s (association phase), followed by 180 s of
524 dissociation. Reference sensors were incubated in buffer alone under identical conditions. Data
525 were reference-subtracted and analyzed using the Octet Analysis Studio (v13.0, Sartorius).

526 **Public antibody analysis**

527 Prefusion-specific gB mAbs (1-14, 5-18, 3-5, 3-6) and prefusion-preferring gB mAbs (1-13, 5-13)
528 were compared against a database of previously published antibodies consisting of 1.7 million
529 paired antibody sequences. This database consists of a previously curated dataset[64], expanded with
530 antibodies from public databases[65-72]. In comparing antibody pairs, V gene paralogues were treated
531 as the same, and CDR3 identity was calculated by employing the Levenshtein distance metric,
532 measuring the difference between amino acid sequences and dividing it by the length of the longer
533 CDR3 region in the pair to obtain sequence identity. Scatterplots in **Extended Data Fig. 2a** depict
534 these pairs of antibodies.

535 **Affinity measurement**

536 For kinetics analyses, HSV-2 IgGs containing an HRV3C protease cleavage site engineered
537 between the CH1 and CH2 domains of the heavy chain were incubated with 5% (w/w) His-tagged
538 HRV3C protease at 4 °C overnight. The reaction mixtures were then passed over Protein A and
539 Ni-NTA resins to remove the cleaved Fc fragment and excess protease. The resulting Fabs were
540 purified by SEC on a Superdex 200 Increase column (Cytiva) equilibrated in PBS. Purified soluble
541 HSV-2 and HSV-1 prefusion-stabilized gB bearing a C-terminal 8xHis-tag were immobilized onto
542 Ni-NTA biosensors (Sartorius) to a response level of approximately 0.7–0.8 nm in HBS-P buffer
543 (10 mM HEPES pH 7.4, 150 mM NaCl, 0.005% v/v Surfactant P20) with 20 mM imidazole and

544 0.1% w/v BSA. After establishing a 180s baseline, the immobilized HSV-2 and -1 gB sensors were
545 dipped into wells containing two-fold serial dilutions of Fabs. Sensors immobilized with gB
546 proteins were run in parallel using buffer-only as a reference control. Dissociation was monitored
547 for 600 s by transferring sensors into buffer-only wells. All data were reference-subtracted and
548 globally fit to a 1:1 binding model using the Octet Analysis Studio (v13.0, Sartorius).

549 **Cryo-EM sample preparation and data collection**

550 Purified HSV-2 prefusion-stabilized gB was mixed in PBS to a final concentration of 4.0 mg mL^{-1}
551 with 1.2-fold molar excess of Fabs 5-18, 1-14, or a combination of 3-5 and 3-6. Complexes were
552 incubated for 30 min at 4 °C before adding 10X CMC CHAPS (VitroEase™ Buffer Screening Kit,
553 Thermo Fisher Scientific) to a final concentration of 0.25X CMC. Immediately after CHAPS
554 addition, 3.0 µL of sample was applied to UltrAuFoil R1.2/1.3 grids (Electron Microscopy
555 Sciences) that had been glow-discharged using a PELCO easiGlow (Ted Pella) for 30 s at 20 mA.
556 Grid vitrification was performed using a Vitrobot Mark IV (Thermo Fisher Scientific) operated at
557 4 °C in 100% humidity. A blot force of 8 was applied for 6 s to remove excess liquid before plunge-
558 freezing the grids into liquid ethane. For data collection, 2,553 movies for the Fab 1-14 complex,
559 2,551 movies for the 5-18 Fab complex, and 3,060 movies for the Fab 3-5/Fab 3-6 complex were
560 collected from single grids using a Glacios TEM (Thermo Fisher Scientific) equipped with a
561 Falcon 4 detector (Thermo Fisher Scientific). Data for the 1-14 and 1-15 complexes were acquired
562 at a 30° stage tilt, whereas data for the 3-5/3-6 complex were collected without tilt. All movies
563 were recorded using SerialEM v4.0.10 automation software[73]. Movies were acquired at a
564 calibrated pixel size of 0.933 Å/pixel (total dose: 49 e^{-}/Å^2). Additional details about data collection
565 parameters are summarized in **Supplementary Table 4**.

566 **Cryo-EM processing and structure determination**

567 Motion correction, CTF estimation, and particle picking were performed using CryoSPARC Live.
568 All subsequent image processing steps were performed in CryoSPARC v4.7.1 and v5.0.0-
569 privatebeta.3[74]. Briefly, particles underwent two rounds of *ab initio* reconstruction and
570 heterogeneous refinement, followed by re-extraction at 384 px. Multiple rounds of non-uniform
571 refinements with optimized parameters were then performed to improve resolution, followed by
572 reference-based motion correction (**Extended Data Fig. 7, 8, 11**). For the Fabs 3-5 and 3-6
573 complex, 3D classification was performed (**Extended Data Fig. 11**). Final map sharpening was
574 performed using EMReady v2.2.2[75] within the SBgrid environment[76]. Initial models were
575 generated by combining the HSV-2 prefusion-stabilized gB structure[42] with Alphafold3-predicted
576 models of the variable regions of 5-18, 1-14, 3-5, and 3-6, produced by inputting their VH and VL
577 sequences (https://alphafoldserver.com)[77]. The highest-confidence output model was docked into
578 the refined cryo-EM map via ChimeraX[78]. Missing residues were manually built in Coot[79], and
579 structures were interactively refined using a combination of Phenix[80], Coot, and ISOLDE[81]. N-
580 acetyl-glucosamine (NAG) and β-mannose (BMA) were added to glycosylation sites and refined
581 using ChimeraX and ISOLDE. Antigen-antibody interfaces and buried surface areas were
582 analyzed using the PDBe PISA service (European Bioinformatics Institute;
583 http://www.ebi.ac.uk/pdbe/prot_int/pistart.html) and ChimeraX. Secondary structure elements
584 were derived from the HSV-2 gB structure in complex with Fabs 3-6 and 3-5, and plotted alongside
585 sequence alignments of HSV-1 and HSV-2 gB generated using the UniProt Clustal Omega server[82].

586 **Plaque reduction neutralization test**

587 Serial dilutions of mAbs were incubated with 75–160 plaque-forming units (PFU) of HSV1-NS or
588 65–120 PFU of HSV2-G for 1 h at 37 ºC and 5% CO_2. This mixture was added to a confluent layer
589 of Vero cells in 6-well plates and incubated for 1 h at 37 ºC and 5% CO_2, with shaking every 15

590 minutes, after which a 1:1 methylcellulose:media overlay was added. The plates were then
591 incubated for 44 to 48 h at 37 ºC and 5% CO_2. Cells were fixed with a 1:1 ethanol:methanol
592 solution for 30 min prior to staining with 12% Giemsa for 24 to 48 h. The stain was then removed,
593 and plaques were counted to determine the extent of neutralization relative to virus-only controls.

594 **Intracellular and extracellular flow cytometric analysis**

595 HEp-2 and HEK293T cell lines were harvested for flow cytometry staining. Cells were incubated
596 with Alexa Fluor 700 NHS ester (succinimidyl ester) (Thermo Fisher Scientific) prior to
597 fixation/permeabilization to enable viability assessment. For extracellular staining, cells
598 were incubated on ice with 25 μg mL^{-1} unlabeled experimental and control IgG mAbs diluted in
599 flow cytometry staining buffer, or flow cytometry staining buffer alone (secondary controls). Cells
600 were washed, and rat anti-human IgG Fc-PE/Cy7 (Biolegend cat no. 410721, clone M1310G05,
601 1:1500) was used to detect human IgG mAbs. For intracellular staining, cells were fixed and
602 permeabilized using the BD Cytofix/Cytoperm kit, followed by incubation with 25 μg mL^{-1}
603 experimental or control mAbs diluted in the kit perm/wash buffer per kit instructions. Cells
604 were washed, and rat anti-human IgG Fc-PE/Cy7 (Biolegend cat no. 410721, clone M1310G05,
605 1:1500) was diluted in perm/wash buffer and used to detect human IgG mAbs. All cells
606 were resuspended in 1% paraformaldehyde, 2 mM EDTA in PBS and stored at 4 °C prior to
607 acquisition on a BD Biosciences LSR Fortessa flow cytometer. Data were analyzed using FlowJo
608 software (BD Biosciences). Gating strategies and IgG^+ plots can be found in **Extended Data Fig.**
609 **6**.

610 **Survival study in a neonatal mouse model**

611 Two-day-old C57BL/6J pups under 1% isoflurane anesthesia were treated with 80 μg of mAb in
612 a 20 μL volume intraperitoneally (i.p.) using a 25 μL Hamilton syringe and then immediately

613 challenged intranasally (i.n.) with 500 PFU of HSV2 CNS11 in a 5 µL volume and monitored for
614 survival for 21 days post-infection. Survival endpoints were defined in accordance with the criteria
615 specified in the IACUC protocol (excessive morbidity such as hunching, spasms and/or paralysis
616 and/or >10% weight loss from the previous measurement). All animal procedures were performed
617 following approval by Dartmouth's Institutional Animal Care and Use Committee and in
618 accordance with Dartmouth's Center for Comparative Medicine and Research policies.

619 **Statistical methods**

620 All statistical analyses were performed using GraphPad Prism version 9.0.0. Results of the
621 challenge study were graphed as a cumulative Kaplan-Meier survival curve, and comparisons
622 between groups were performed using a log-rank (Mantel-Cox) test. *In vitro* neutralization curves
623 were generated by fitting data points using a variable slope and a four-parameter regression curve
624 (best-fit method). ELISA data were analyzed using variable slope and a four-parameter regression
625 curve, with area under the curve (AUC) reported from log-transformed values. The number of
626 replicates per experiment is indicated in the figure legends. No data or experiments were excluded
627 unless there were technical issues with the experiment, and outliers were not excluded. Exact P
628 values are denoted in the figures.

FIGURES

a

Name	Native Isotype	VH Gene	CDRH3	CDRH3 Length	VL Gene	CDRL3	CDRL3 Length	LIBRA-seq Score (LSS) HSV-2 Prefusion gB	LIBRA-seq Score (LSS) HSV-2 Postfusion gB
1-9	IGHG1	IGHV3-74	TRSSVSGTFPFDF	13	IGLV3-21	QVWDSNSDHVV	11	1.42	1.13
1-10	IGHG1	IGHV5-51	ARQGFFYNGAGTYSQAFDY	19	IGKV3-20	QLYGDSPTWT	10	1.37	1.02
1-11	IGHG3	IGHV3-7	ARDAFYLDLDH	11	IGLV1-40	QSFDSSLSGRV	11	1.28	1.54
1-12	IGHG1	IGHV5-51	ARQGYFYYGGGTYSQAFDY	19	IGKV3-20	QLYGNSPTWT	10	1.33	1.01
1-13	IGHG1	IGHV3-23	TKADRMATRLYYFDH	15	IGKV1-5	QQYNSYSYT	9	1.31	0.40
1-14	IGHG1	IGHV3-30	GRVARQFLENVYVDM	15	IGKV3-15	QHYHTWPPS	9	1.24	-1.03
1-15	IGHG1	IGHV5-51	MAGGYYDSGNL	11	IGKV2-28	MQVLQTPLT	9	1.05	0.76
1-16	IGHG1	IGHV1-2	ARLLGFKKFYDNSGYHTP	18	IGLV1-40	QSYDYRLSGWV	11	0.24	1.73
1-17	IGHG1	IGHV1-2	ARDLARTDEIVGPFKWFDP	19	IGLV1-40	QSYDHSLGGSV	11	0.01	1.62
3-5	IGHG1	IGHV4-4	ARDSGTYFDY	10	IGLV2-14	SSHSSSSTRVV	11	1.36	-1.19
3-6	IGHG1	IGHV3-30	ARDAMWEWSGGAGYYRFYGMDV	22	IGLV1-44	GAWDDSQSGFFV	12	1.23	-1.19
3-7	IGHG1	IGHV3-53	ARVGGGTSGPLDY	13	IGLV3-21	QVWDRSSGHLV	11	1.34	1.15
3-8	IGHG1	IGHV3-73	ARHATDSASGSFDF	14	IGLV3-21	QVWDNSSDQGV	11	1.25	1.12
3-11	IGHG2	IGHV4-30	ARTGGCSGVNCPSGYTDF	18	IGLV3-21	QVWDSGQV	8	1.26	1.12
5-12	IGHG1	IGHV1-18	ARGGGSAALPHAFDI	15	IGKV1-5	QQYHDFPWT	9	2.21	1.15
5-13	IGHG1	IGHV3-7	ARDTLMTIDY	10	IGLV2-8	SSYAGSNNLYV	11	2.63	-0.37
5-14	IGHG1	IGHV1-46	ARSVMATVPYDY	12	IGKV1-39	QQSYNTLPIT	10	1.63	0.54
5-15	IGHG1	IGHV3-23	ARDELPSTVFDY	12	IGLV4-69	QSWGKGIYAV	10	1.56	0.83
5-16	IGHG1	IGHV4-59	ARGRLTATIPVDH	13	IGKV1-33	QQYDGLPYT	9	1.95	0.59
5-18	IGHM	IGHV4-39	ARVGGLTTVVTPVDY	15	IGKV1-5	QHYNSYSGT	9	3.14	-1.65
5-20	IGHA1	IGHV4-31	ASDLGGIHD	9	IGKV1-39	QQSDSVPIT	9	0.30	1.13
5-21	IGHA1	IGHV1-2	ARELFREDYYDKIGCFDP	18	IGLV1-40	QSYDISLSGSV	11	0.23	1.47

b

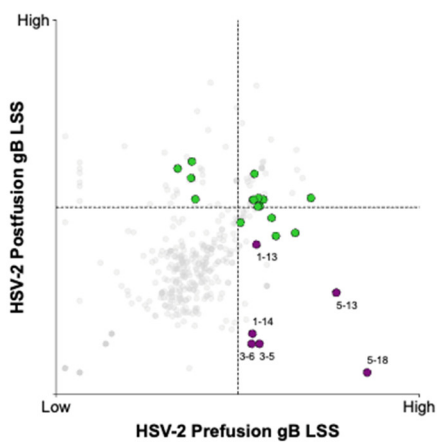

c

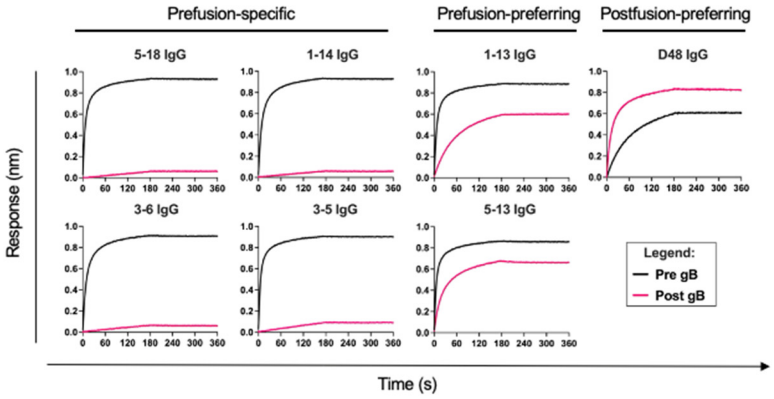

Figure 1. Identification and characterization of HSV-2 prefusion-specific human antibodies. **a**, Sequence properties of HSV-2 gB antibodies identified by LIBRA-seq. The complementarity-determining region (CDR) sequences and lengths for each antibody are shown at the amino acid level. LIBRA-seq scores (LSS) for the selected antibodies to HSV-2 pre- and postfusion gB antigens are shown as a heat map from –2 (tan) to 0 (white) to 2 (purple); scores outside of this range are shown as the minimum and maximum values. **b**, LIBRA-seq scores for each recovered B cell are plotted, with cutoffs set at an LSS of 1. Antibodies encoded by B cells colored in purple were selected for experimental validation. The remaining 22 selected antibodies are colored green. **c**, BLI sensorgrams for immobilized IgGs binding to prefusion-stabilized HSV-2 gB (black) or postfusion HSV-2 gB (pink).

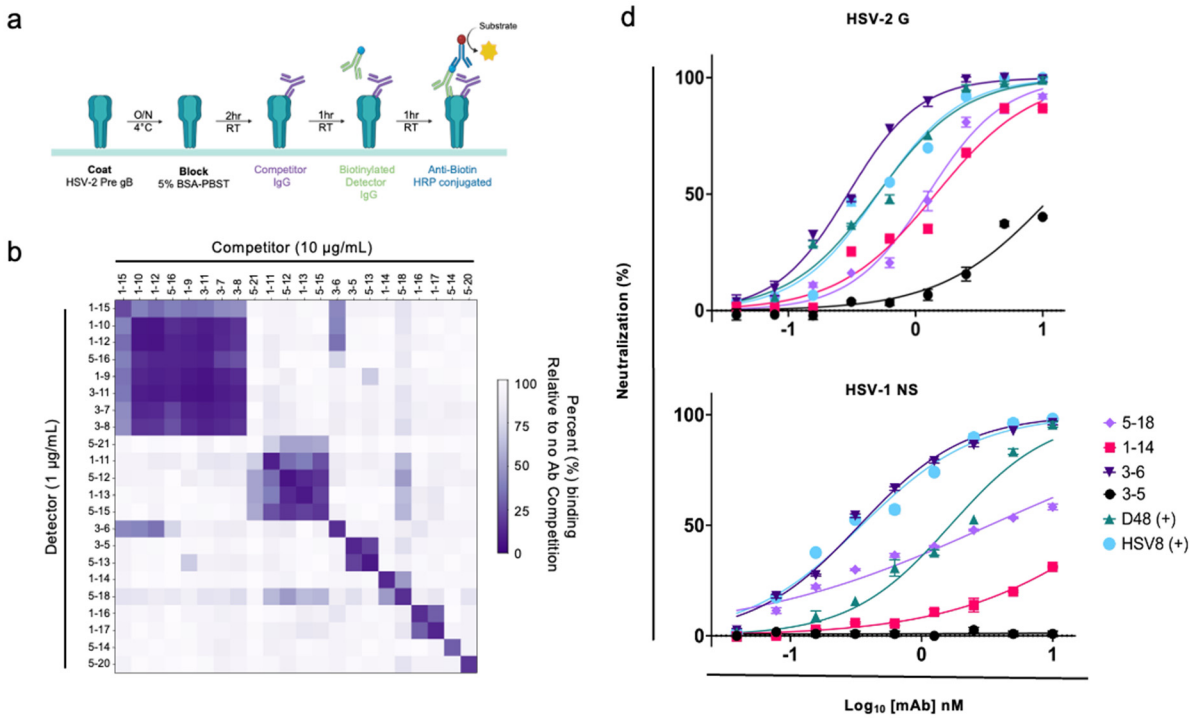

c

Specificity	Fab	HSV-2 Prefusion gB		HSV-1 Prefusion gB	
		Kd (nM)	Dissociation Rate Constant (k_{off})	*Kd* (nM)	Dissociation Rate Constant (k_{off})
Prefusion-specific	5-18	0.20	1.8×10^{-4} s^{-1}	40.00	2.3×10^{-3} s^{-1}
	1-14	0.03	1.2×10^{-5} s^{-1}	0.12	1.1×10^{-5} s^{-1}
	3-6	0.12	5.3×10^{-5} s^{-1}	0.08	7.5×10^{-5} s^{-1}
	3-5	0.15	8.2×10^{-5} s^{-1}	0.04	4.3×10^{-5} s^{-1}
Prefusion-preferring	1-13	0.11	9.9×10^{-5} s^{-1}	3.20	1.1×10^{-4} s^{-1}
	5-13	0.17	6.1×10^{-5} s^{-1}	0.21	1.1×10^{-4} s^{-1}

e

	1-14	3-5	3-6	5-18	D48 (+)	HSV8 (+)
HSV2-G	1.44	12.32	0.29	1.25	0.50	0.51
HSV1-NS	>	>	0.34	3.30	1.66	0.35

> 15 nM
5 - 15 nM
1.1 - 5 nM
< 1 nM

Figure 2. Binding and neutralization of prefusion-specific gB antibodies. a, ELISA-based antibody-antibody binding competition assay (schematic created using Biorender.com). **b**, The percentage of binding remaining in the presence of a competitor mAb is shown for each mAb, with darker colors corresponding to stronger competition between the given pair of mAbs. Dark purple clusters indicate a group of mAbs targeting overlapping epitopes on the HSV-2 prefusion gB antigen. **c**, Equilibrium dissociation constants (K_d) and dissociation rate constants (k_d) of gB Fabs binding to immobilized HSV-2 prefusion gB on Ni^{2+}-NTA biosensors. **d**, Neutralization profiles of gB-specific mAbs against HSV-2 G and HSV-1 NS strains detected by a plaque reduction assay. **e**, Neutralization midpoint concentration (IC_{50}) summary heatmap, with strong neutralization of HSV-2 G and HSV-1 NS (< 1 nM) shown in dark purple and weak/non-neutralizing (> 15 nM) shown in light purple. Calculated by non-linear regression analysis using GraphPad Prism software.

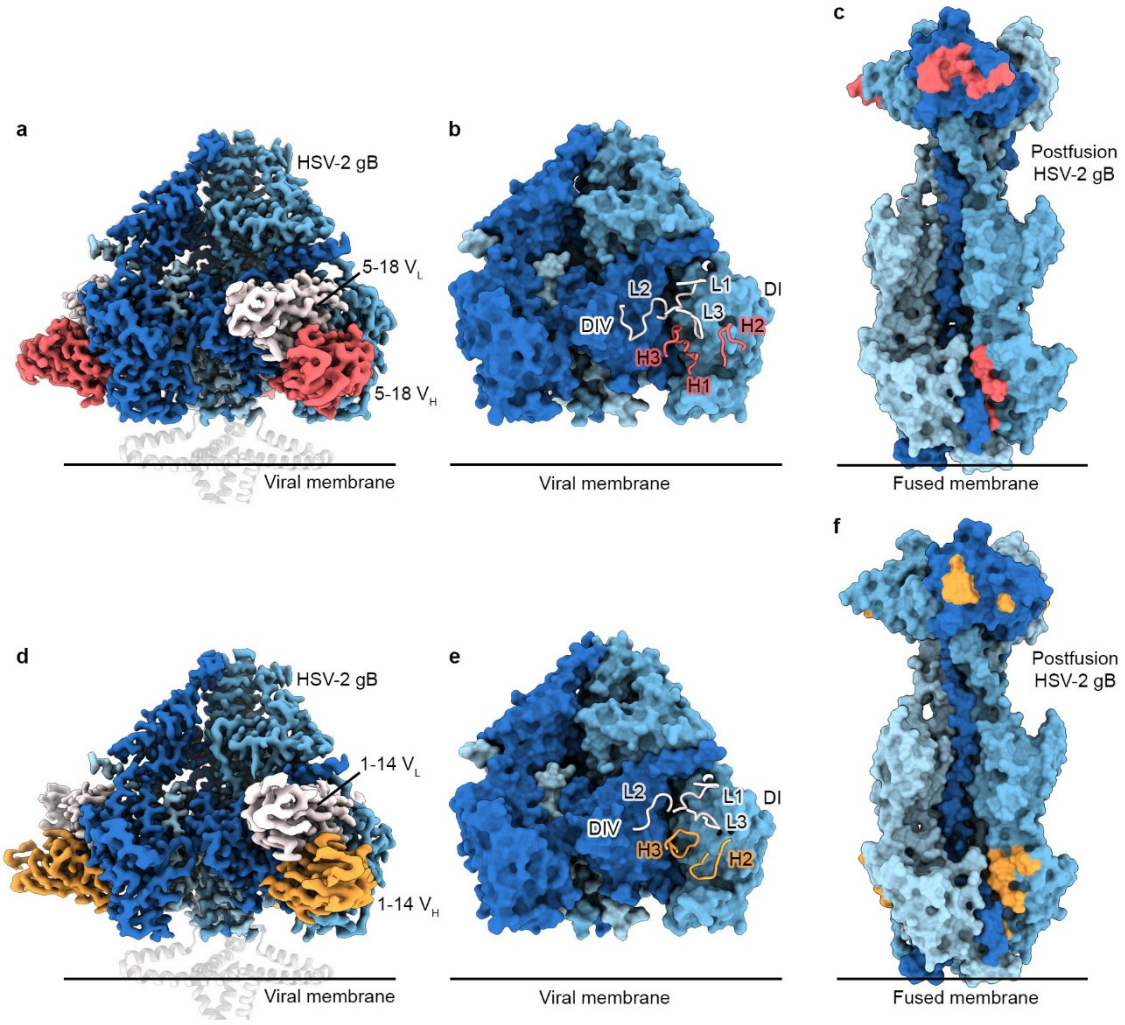

Figure 3. Fabs 5-18 and 1-14 recognize prefusion-specific quaternary epitopes spanning domains I and IV. a, Cryo-EM map side view of Fab 5-18 bound to the HSV-2 prefusion gB trimer. The 5-18 V_H is colored red, and the V_L is colored white. Each prefusion gB protomer is colored a different shade of blue. The MPR and TM regions from PDB ID: 9Q9L are shown as transparent helices, and a horizontal black line indicates the approximate position of the viral membrane. **b**, Side view of prefusion HSV-2 gB depicted as a molecular surface with the 5-18 CDRs depicted as ribbons. Domain I (DI) and domain IV (DIV) are labeled on gB. **c**, Side view of postfusion HSV-2 gB (PDB ID: 8RH2) shown as a molecular surface with the 5-18 epitope colored red. The fused membrane is indicated by a horizontal black line. **d**, **e**, and **f**, are the same as (a), (b), and (c), but depict the Fab 1-14 complex, CDRs, and epitope.

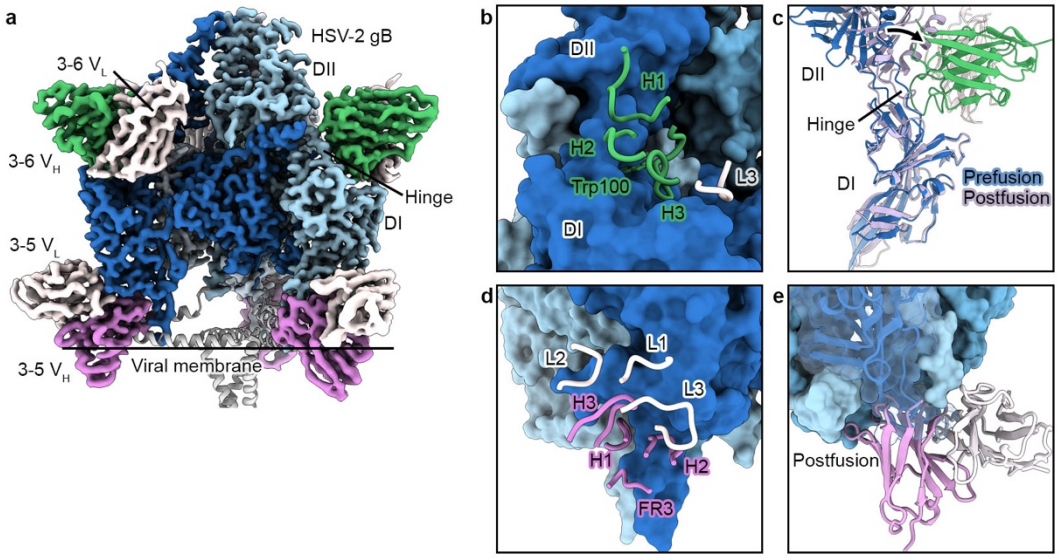

Figure 4. Antibodies 3-6 and 3-5 bind distinct prefusion-specific epitopes located within a single protomer. a, Cryo-EM map side view of Fabs 3-6 and 3-5 bound to the HSV-2 prefusion gB trimer. The 3-6 V_H is colored green, the 3-5 V_H is colored magenta, and both V_Ls are colored white. Each prefusion gB protomer is colored a different shade of blue. The MPR and TM regions from PDB ID: 9Q9L are shown as white helices, and a horizontal black line indicates the approximate position of the viral membrane. **b**, Magnified view of prefusion HSV-2 gB depicted as a molecular surface with the 3-6 CDRs depicted as ribbons. Domain I (DI) and domain II (DII) are labeled on gB. The sidechain of Trp100 in the HCDR3 (H3) is shown as sticks. **c**, Superimposition of DI from the 3-6-bound prefusion gB monomer and a monomer from postfusion gB (PDB ID: 8RH2) showing the rearrangement of DII (indicated with a black arrow) that blocks Fab 3-6 binding. **d**, Magnified view of prefusion HSV-2 gB depicted as a molecular surface with the 3-5 CDRs and framework 3 (FR3) region depicted as ribbons. **e**, Magnified view of a superposition of the postfusion gB trimer (PDB ID: 8RH2) and Fab 3-5, with one protomer surface rendered transparent and the chain shown as ribbons. In the postfusion conformation, gB cannot bind Fab 3-5 due to numerous clashes.

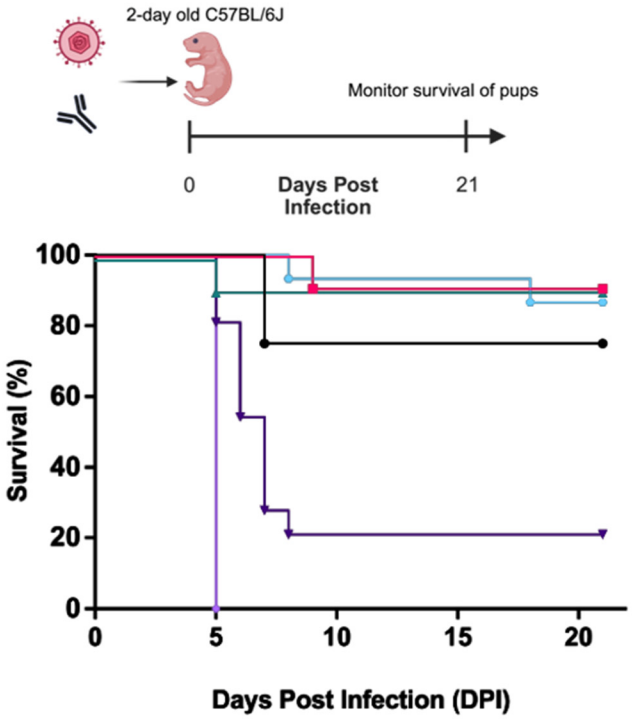

mAb	Overall Survival Proportions (%)	P-value compared to VRC01 control
3-6	90.91	0.0002
5-18	75.00	0.0001
1-14	20.00	0.0020
D48	86.67	<0.0001
HSV8	90.91	0.0009
VRC01	0.00	-

Figure 5. Prefusion-specific gB antibodies protect from viral challenge in a neonatal mouse model. Overall survival of 2-day old C57BL/6J mice infected intranasally with 500 plaque-forming units (PFU) of HSV-2-CNS11 and treated intraperitoneally with 80 µg monoclonal antibody IgG1 (3-6: n=11, 5-18: n=12, 1-14: n=15, D48: n=15, HSV8: n=11, VRC01: n=9) as shown on the experimental timeline (schematic created using Biorender.com). Statistical significance between the negative control VRC01 mAb and experimental antibodies was calculated by log(rank) (Mantel-Cox) test. Summary table with the overall survival proportions for each experimental group at 21 days post-infection as determined by the survival analysis Kaplan-Meier test.

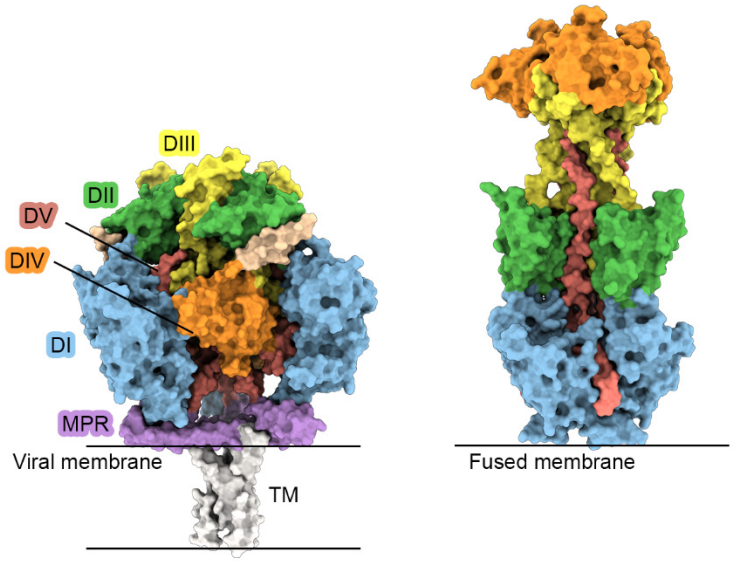

Supplementary Figure 1. Structural comparison of prefusion and postfusion gB. Side views of prefusion (PDB ID: 9Q9L) and postfusion (PDB ID: 9IH8) HSV-2 gB are shown as molecular surfaces. Domain (D) I is colored blue, DII is colored green, DIII is colored yellow, DIV is colored orange, DIV is colored red, and the membrane proximal region (MPR) is colored purple.

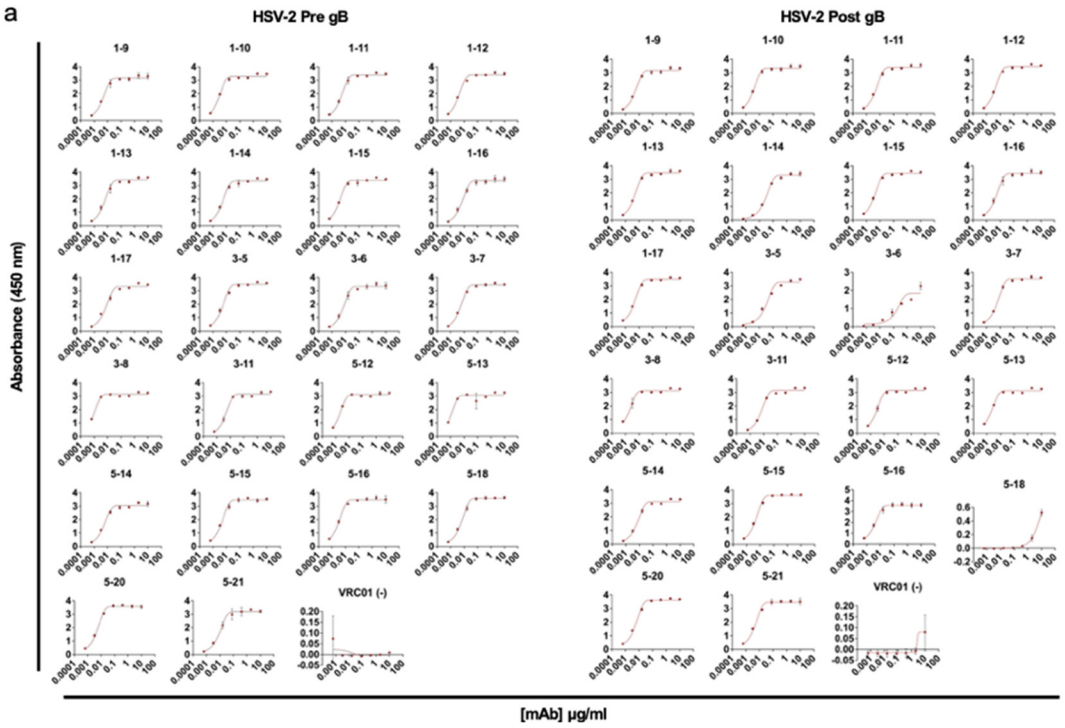

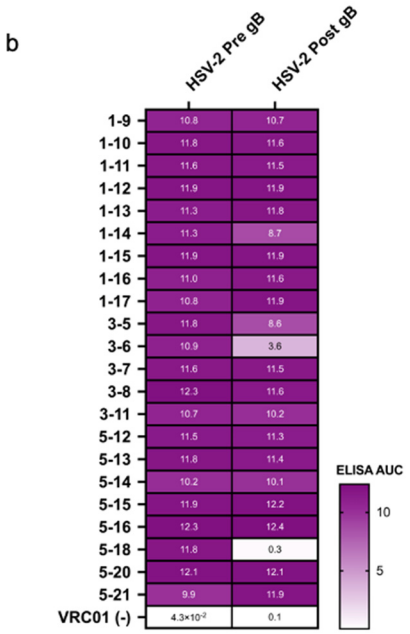

Extended Data Figure 1. Antibodies discovered by LIBRA-seq bind to HSV-2 pre- and postfusion gB. a, Indirect ELISA absorbance measurement of recombinantly produced antibodies binding to HSV-2 prefusion or postfusion gB. **b**, Area under the curve (AUC) of transformed absorbance values. Experiments were performed in technical and biological duplicates.

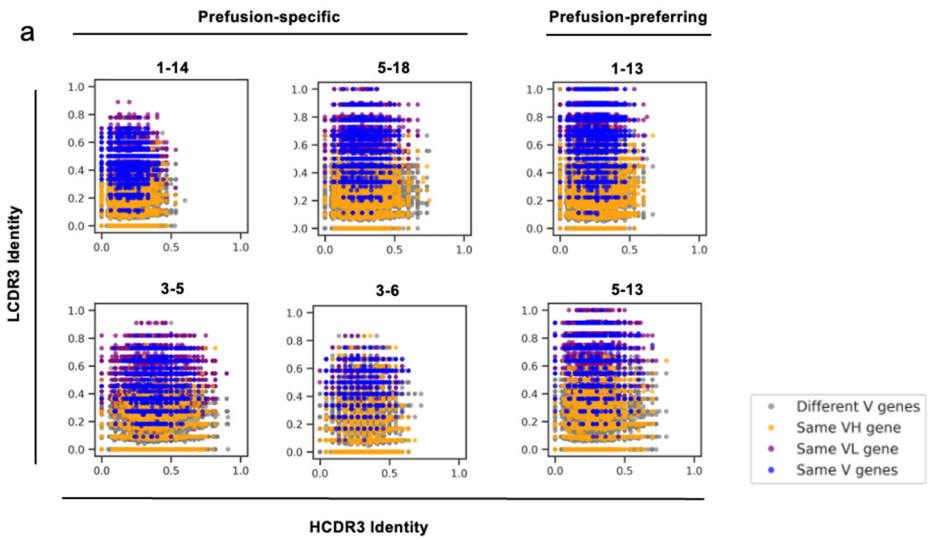

b

Summary counts of prefusion gB mAbs compared to database mAbs

mAb	HCDR3 ≥ 0.7	LCDR3 ≥ 0.7	HCDR3 + LCDR3 ≥ 0.7	Same VH gene	Same VL gene	Same VH + VL gene	VH Clones	Full Clones
1-13	0	45100	0	161443	81710	12390	0	0
1-14	0	388	0	129725	90365	9321	0	0
5-13	163	21090	4	81085	34635	2159	16	1
3-5	4498	4673	22	59763	95923	3258	203	0
3-6	2	538	0	134960	51924	4086	0	0
5-18	20	12307	0	85880	88942	5158	5	0

Extended Data Figure 2. Comparison of prefusion gB mAbs to published antibodies. **a**, Sequence similarity of prefusion gB mAbs to a public database of 1.7 million paired antibody sequences. Each point represents an antibody from the database, compared with the prefusion gB mAb (represented by the title for each panel). Characterized by their identities in the CDR3 of the heavy chain (represented on the x-axis) and the light chain on the y-axis. The color coding of each dot in the plots corresponds to the matching of V genes between pairs of antibodies: Blue dots indicate identical use of both V_H and V_L genes; orange signifies matching V_H gene use; purple represents matching V_L gene use; and gray denotes cases in which neither V_H nor V_L genes match. **b**, Shown are the counts based on comparisons shown in panel (a). Full clones are defined as having matching V-gene usage and ≥ 0.7 CDR3 identity.

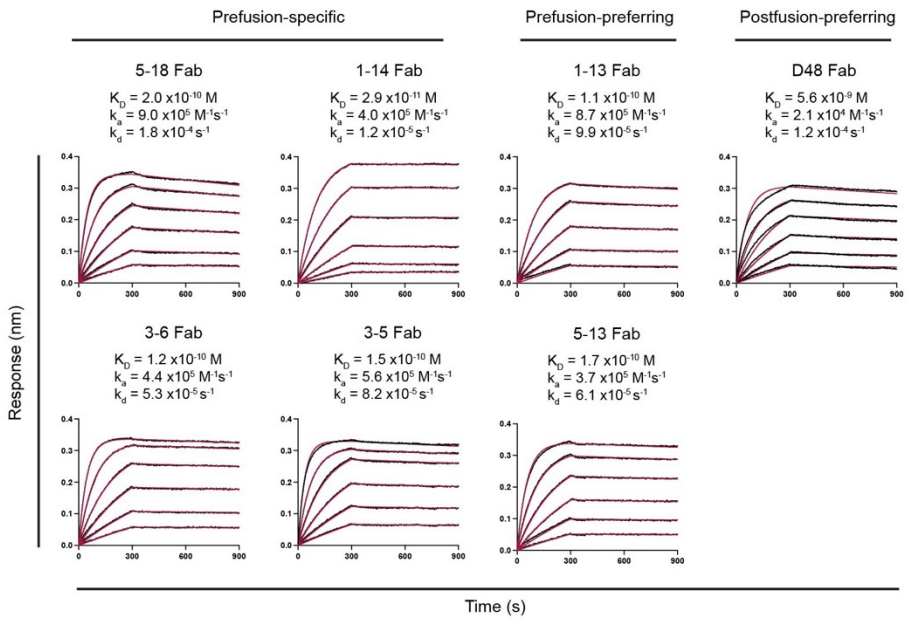

Extended Data Figure 3. Kinetics of isolated Fabs binding to HSV-2 prefusion-stabilized gB. BLI sensorgrams for the association and dissociation kinetics of prefusion-specific and prefusion-preferring Fabs, as well as the postfusion-preferring control Fab D48, binding to HSV-2 prefusion-stabilized gB. Experimental data (black) were globally fit to a 1:1 binding model, with the fitted curves shown in red. The calculated values for K_d, k_a, and k_d are listed above each curve.

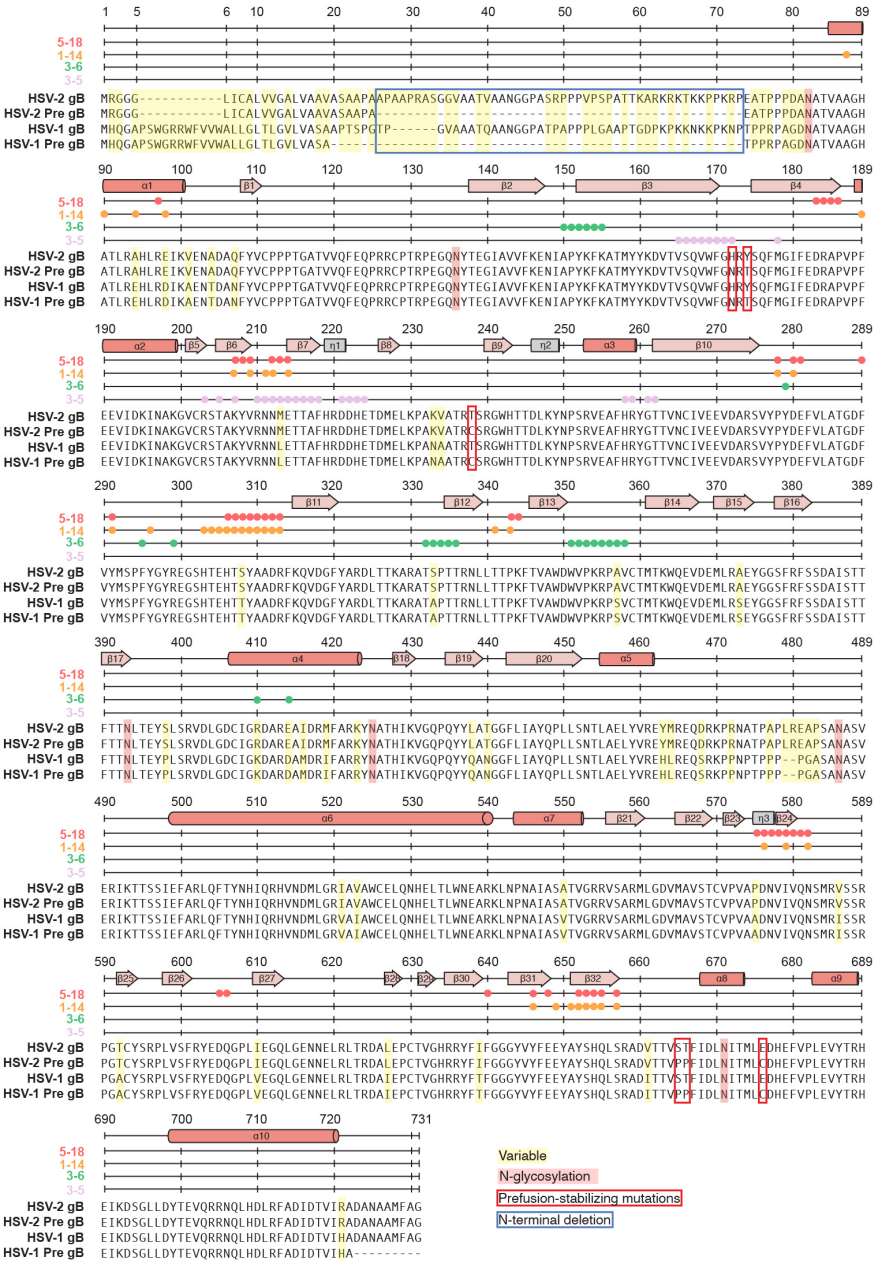

Extended Data Figure 4. Sequence alignment of HSV-2 and HSV-1 gB. Sequence alignment of HSV-2 gB ectodomain residues 1–731 and HSV-1 gB ectodomain residues 1–725. Residues involved in antibody interactions are indicated by colored circles above the alignment. Secondary structure elements were derived from the coordinates of HSV-2 gB bound to Fabs 3-5 and 3-6 and are annotated above the alignment. Variable positions between HSV-2 and HSV-1 gB are highlighted in yellow, *N*-linked glycosylation sites are in red, prefusion-stabilizing substitutions are annotated by red boxes, and the engineered N-terminal deletion is indicated by a blue box.

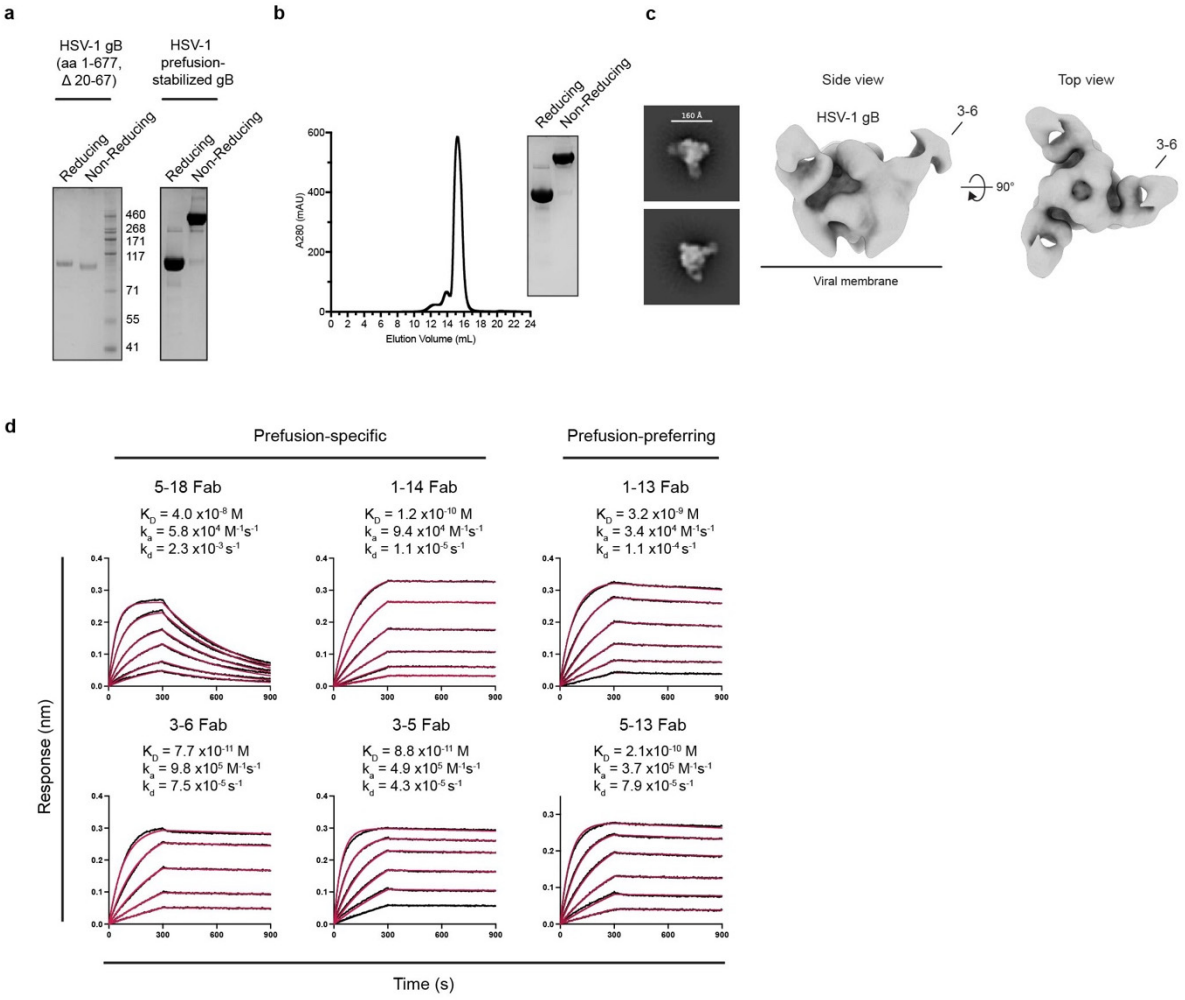

Extended Data Figure 5. Stabilization of HSV-1 prefusion gB and binding of prefusion-specific antibodies. a, SDS-PAGE of HSV-1 gB constructs under reducing and non-reducing conditions. The stabilizing interprotomeric disulfide bond shifts the band to a molecular weight consistent with that of a trimer. **b**, Size-exclusion chromatography (SEC) trace of prefusion-stabilized HSV-1 gB and SDS-PAGE of pooled SEC fractions under reducing and non-reducing conditions. **c**, Negative-stain electron microscopy 2D-class averages and 3D-reconstruction volumes of HSV-1 prefusion-stabilized gB complexed with Fab 3-6. **d**, BLI sensorgrams for the association and dissociation kinetics of prefusion-specific and prefusion-preferring Fabs binding to immobilized HSV-1 prefusion-stabilized gB on Ni^{2+}-NTA biosensors. Experimental data (black) were globally fit to a 1:1 binding model, with the fitted curves shown in red. The calculated values for the K_D, k_a, and k_d are listed above each curve.

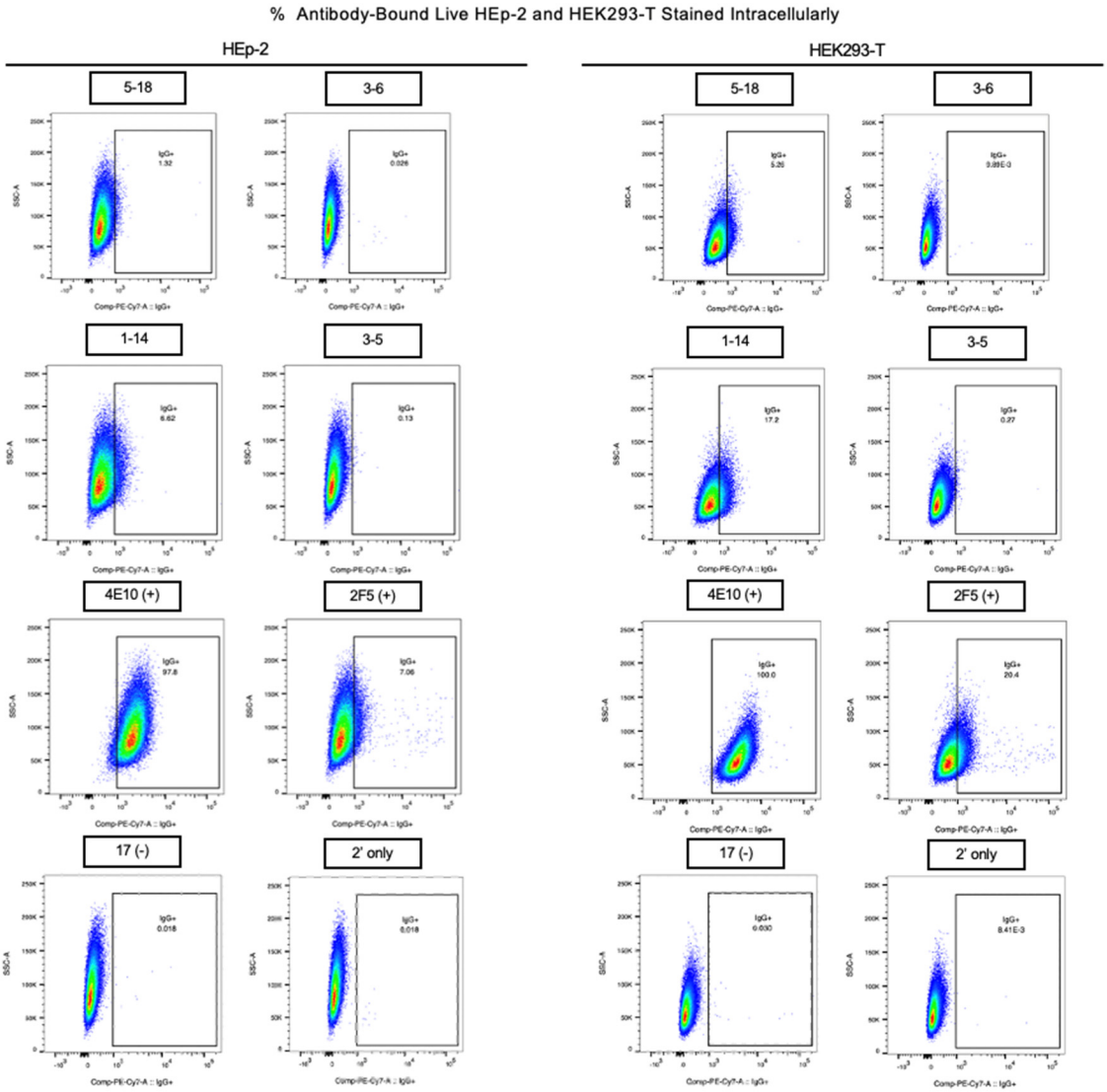

Extended Data Figure 6. Flow cytometry plots of intracellular self-antigen recognition by prefusion-specific mAbs. Representative flow cytometry plots for intracellular staining of HEp-2 cells and HEK293-T cells with 25 µg mL^{-1} positive control mAbs 4E10 and 2F5, negative control 17B, or experimental mAbs 5-18, 3-6, 1-14, and 3-5. Anti-human IgG Fc-PE/Cy7 was used to detect experimental and control recognition of cellular autoantigens.

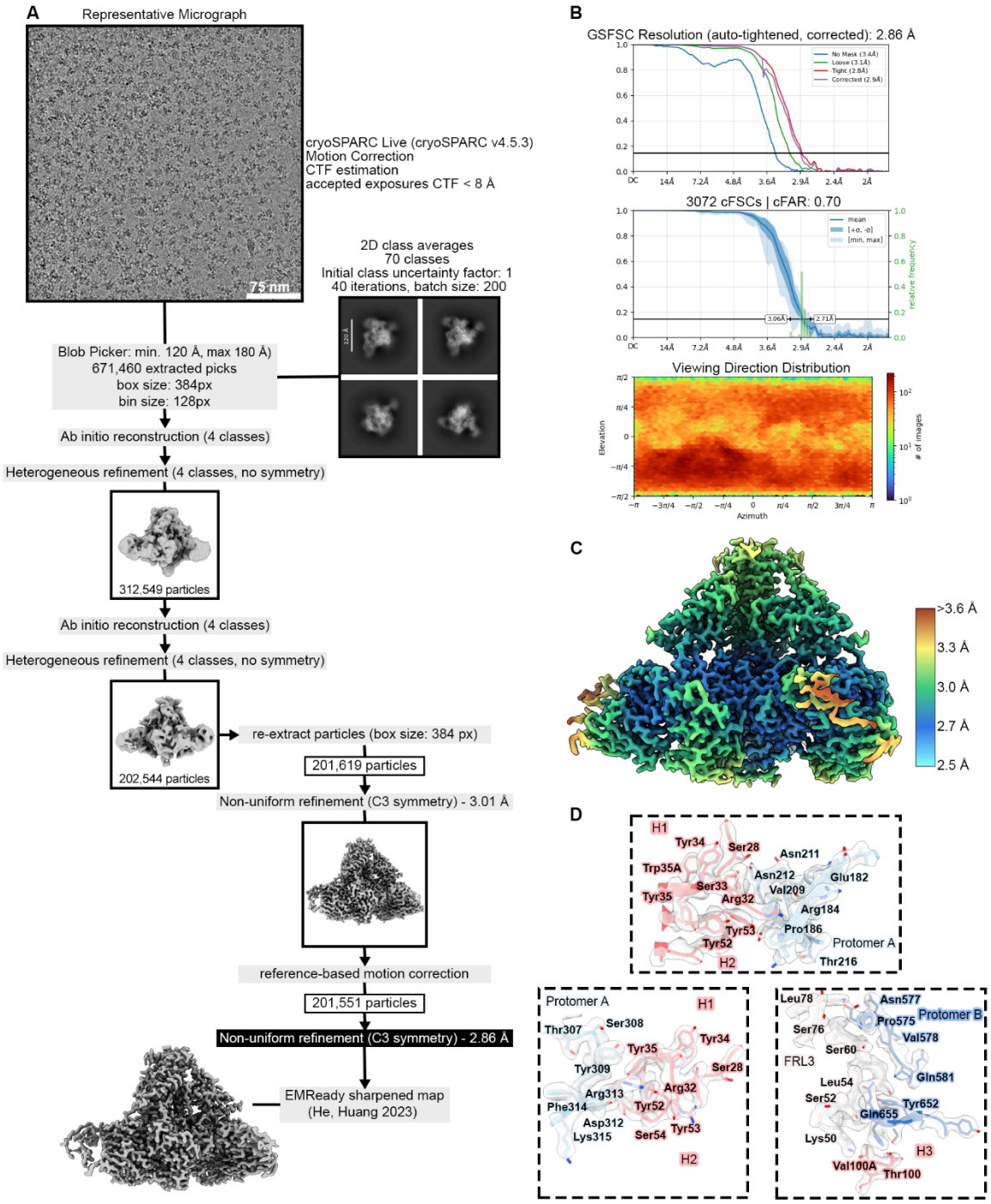

Extended Data Figure 7. Cryo-EM data processing workflow and structure validation for prefusion HSV-2 gB bound to Fab 5-18.

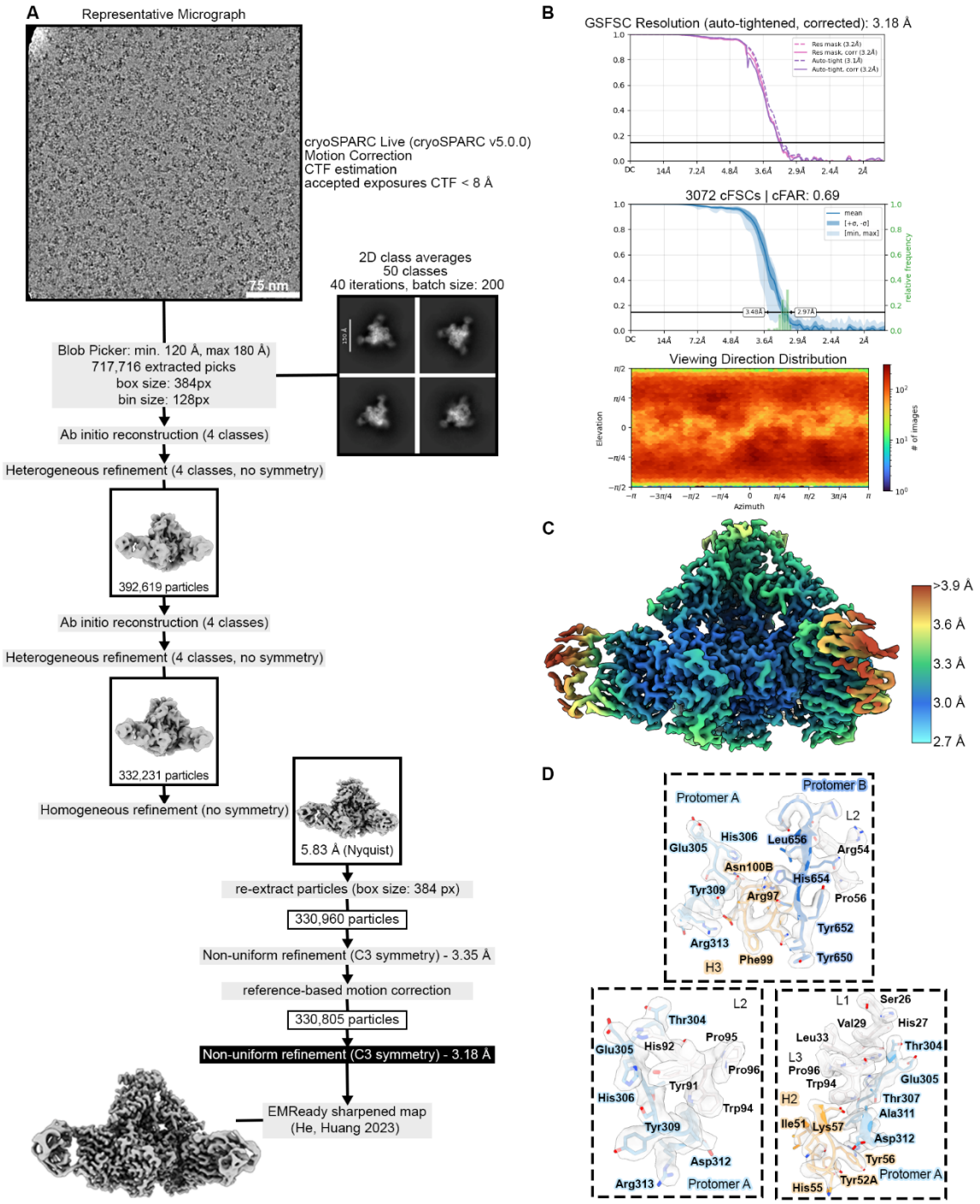

Extended Data Figure 8. Cryo-EM data processing workflow and structure validation for prefusion HSV-2 gB bound to Fab 1-14.

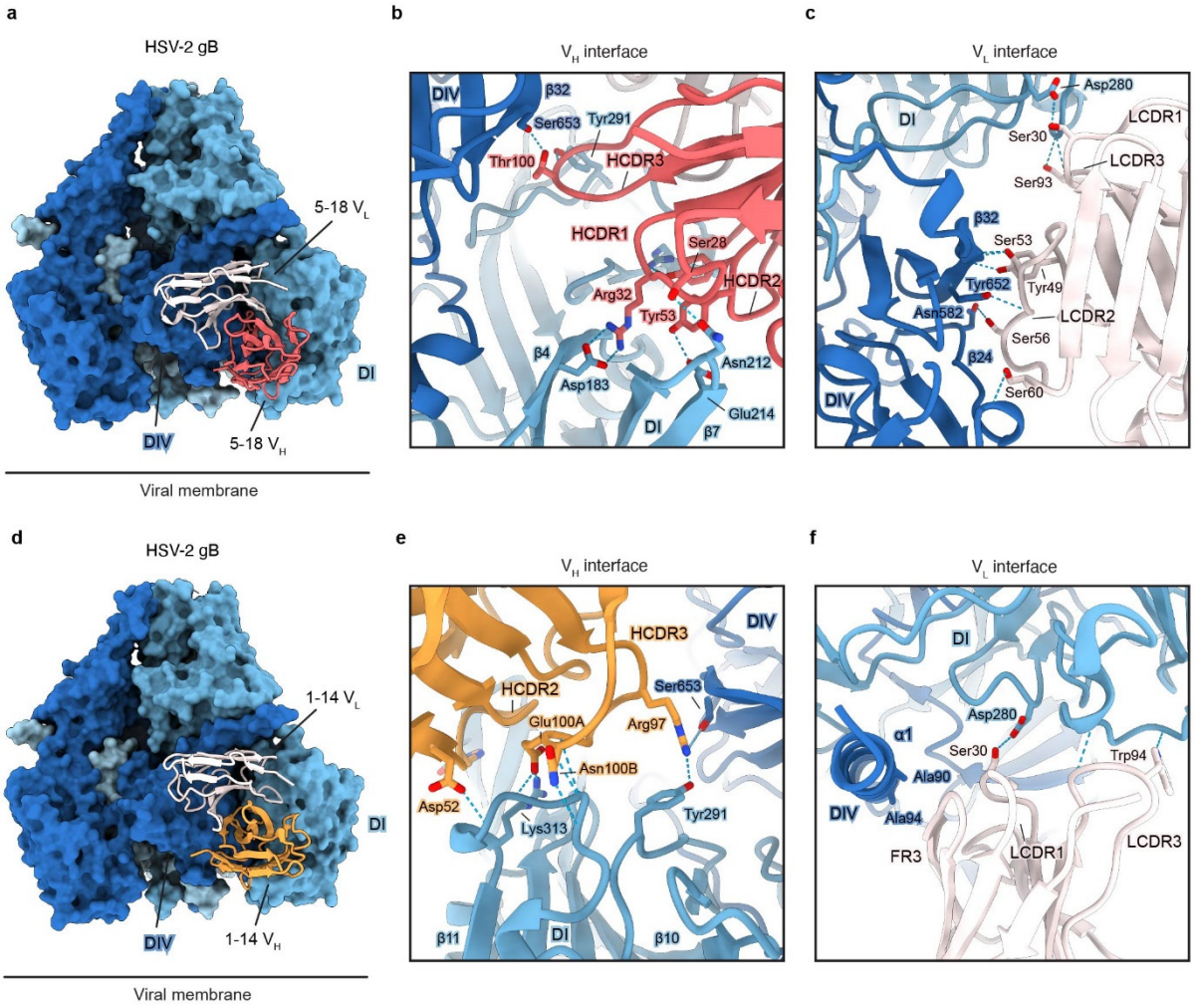

Extended Data Figure 9. Quaternary interfaces of prefusion-specific Fabs 5-18 and 1-14. **a**, Side view of prefusion HSV-2 gB with one bound Fab 5-18. A horizontal black line indicates the approximate position of the viral membrane. **b,** Magnified view of the 5-18 V_H interface spanning Domain (D) I and DIV, depicted as ribbons. HCDR1 and HCDR2 contact DI through multiple hydrogen bonds and salt bridges, with $Arg32_{HCDR1}$ extending to engage the Asp183 sidechain in β4. HCDR3 spans DI and DIV, with $Thr100_{HCDR3}$ forming hydrogen bonds to Tyr291 in DI and Ser653 in DIV. **c**, Magnified view of the 5-18 V_L interface spanning DI and DIV, depicted as ribbons. LCDR1 and LCDR3 interact with DI, whereas LCDR2 engages β24 and β32 in DIV, forming a continuous hydrogen bond network. **d**, Side view of prefusion HSV-2 gB with one bound Fab 1-14. **e**, Magnified view of the 1-14 V_H interface spanning DI and IV, depicted as ribbons. HCDR2 and HCDR3 mediate most contacts with the β10–β11 loop in DI. HCDR3 crosslinks DI and DIV, with $Arg97_{HCDR3}$ forming a hydrogen bond with the sidechain of Tyr291 in DI and Ser653 in DIV. **f**, Magnified view of the 1-14 V_L interface spanning DI and DIV, depicted as ribbons. LCDR1 and LCDR3 contact DI, whereas LCDR2 and FR3 make limited interactions with DIV, including the N-terminal α1 helix.

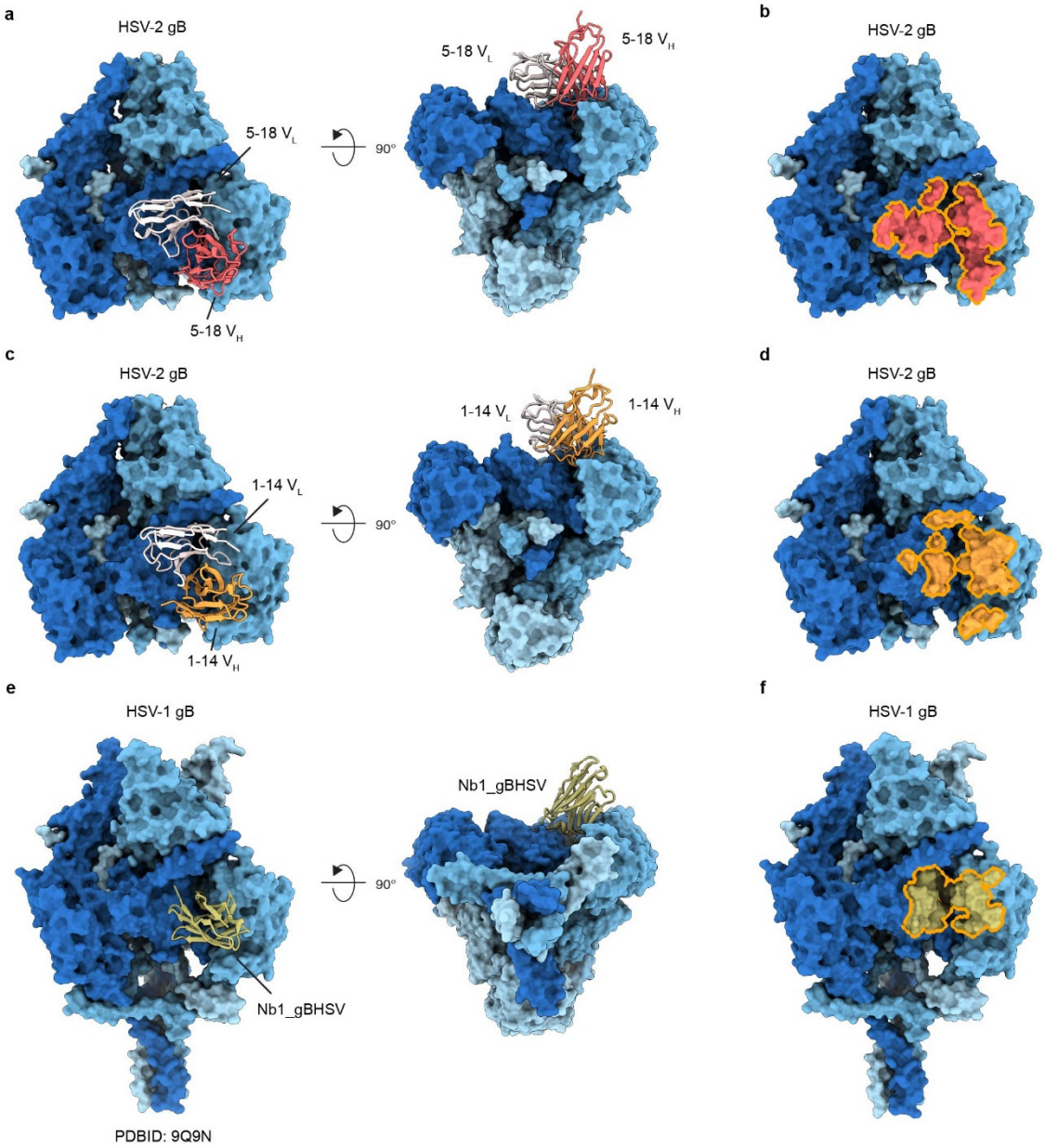

Extended Data Figure 10. Structural comparison of prefusion-specific Fabs 5-18, 1-14, and nanobody Nb1_gBHSV. a, Side (*left*) and bottom (*right*) views of prefusion HSV-2 gB bound to Fab 5-18. **b**, Side view showing the Fab 5-18 epitope footprint outlined in orange. **c**, Side (*left*) and bottom (*right*) views of prefusion HSV-2 gB bound to Fab 1-14. **d**, Side view showing the Fab 1-14 epitope footprint. **e**, Side (*left*) and bottom (*right*) views of prefusion HSV-1 gB bound to nanobody Nb1_gBHSV (PDBID: 9Q9N). **f**, Side view showing the Nb1_gBHSV epitope footprint**.**

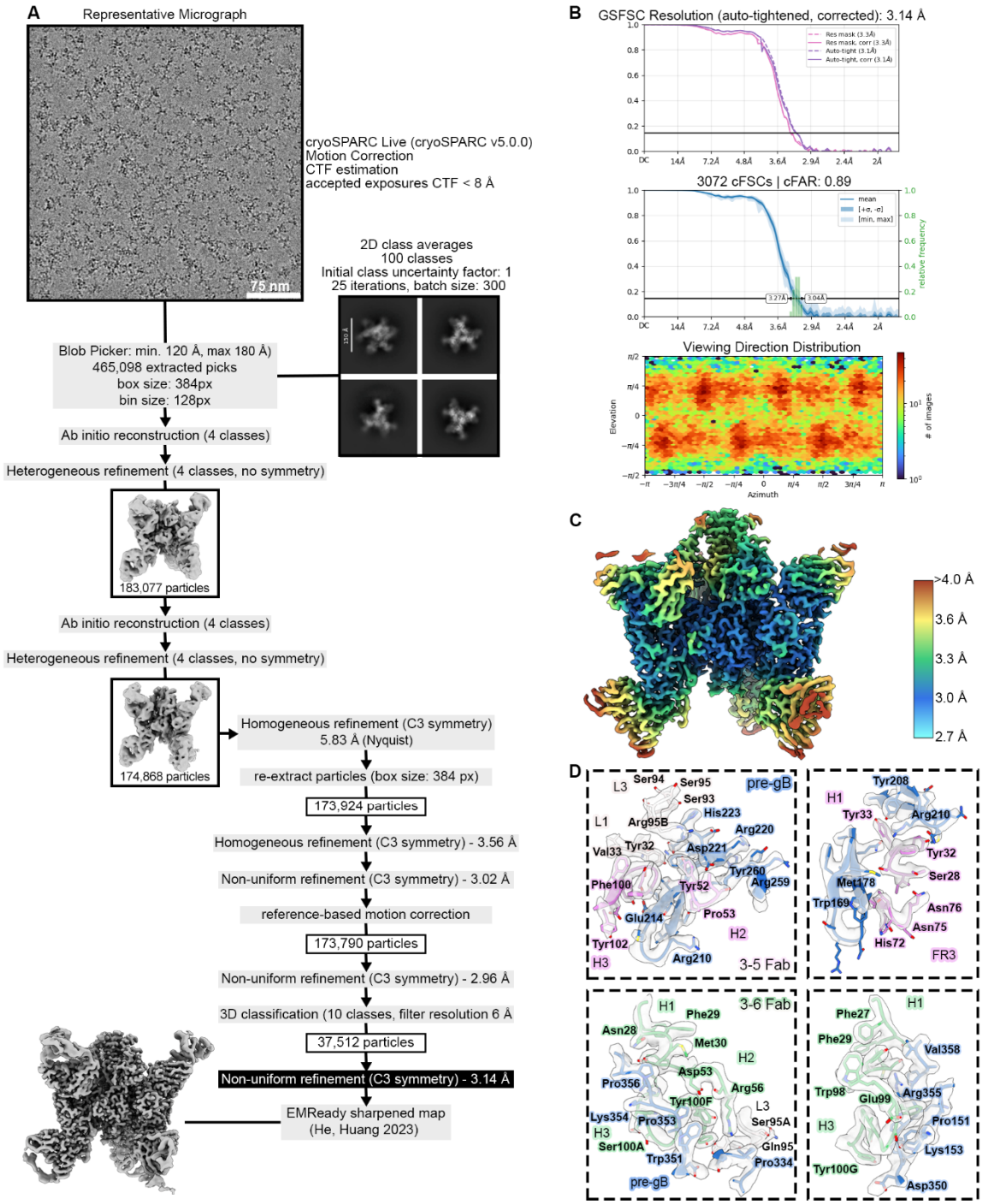

Extended Data Figure 11. Cryo-EM data processing workflow and structure validation for prefusion HSV-2 gB bound to Fabs 3-6 and 3-5.

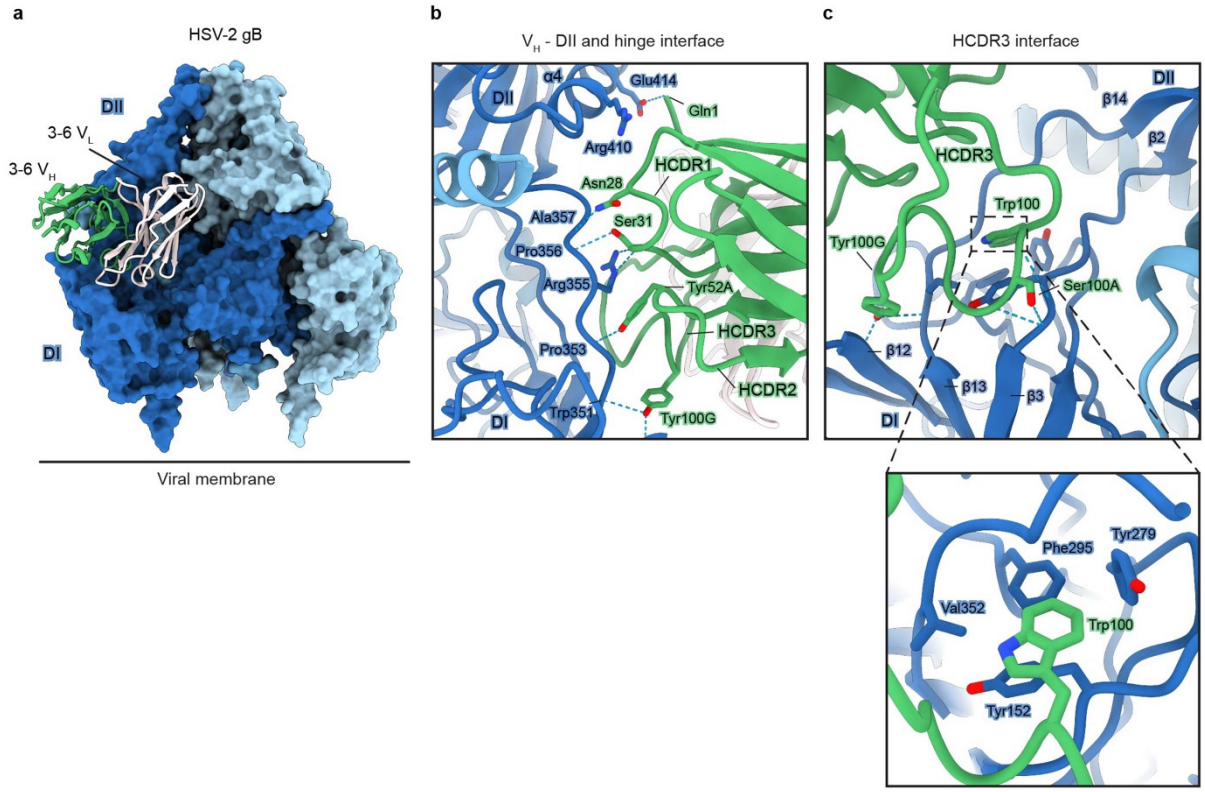

Extended Data Figure 12. Interface of prefusion-specific Fab 3-6 with prefusion HSV-2 gB. **a**, Side view of prefusion HSV-2 gB with one bound Fab 3-6. The 3-6 V_H is colored green, the 3-6 V_L is colored white, and each protomer of prefusion gB is colored in a different shade of blue. A horizontal black line indicates the approximate position of the viral membrane. **b**, Magnified view of the 3-6 V_H interface with the domain (D)II and hinge region, depicted as ribbons. FR1 and HCDR1 of the heavy chain interact with the α4 helix of DII. HCDR1, HCDR2, and HCDR3 form hydrogen bonds with mainchain atoms in hinge residues 351–358 and the sidechain of Arg355. **c**, Magnified view of HCDR3 interactions with DI, depicted as ribbons. HCDR3 contacts β2–β3 loop, β12, and the β13–β14 loop (hinge). The inset shows $Trp100_{HCDR3}$ inserted into a hydrophobic pocket formed by Tyr152, Tyr279, Phe295, and Val352.

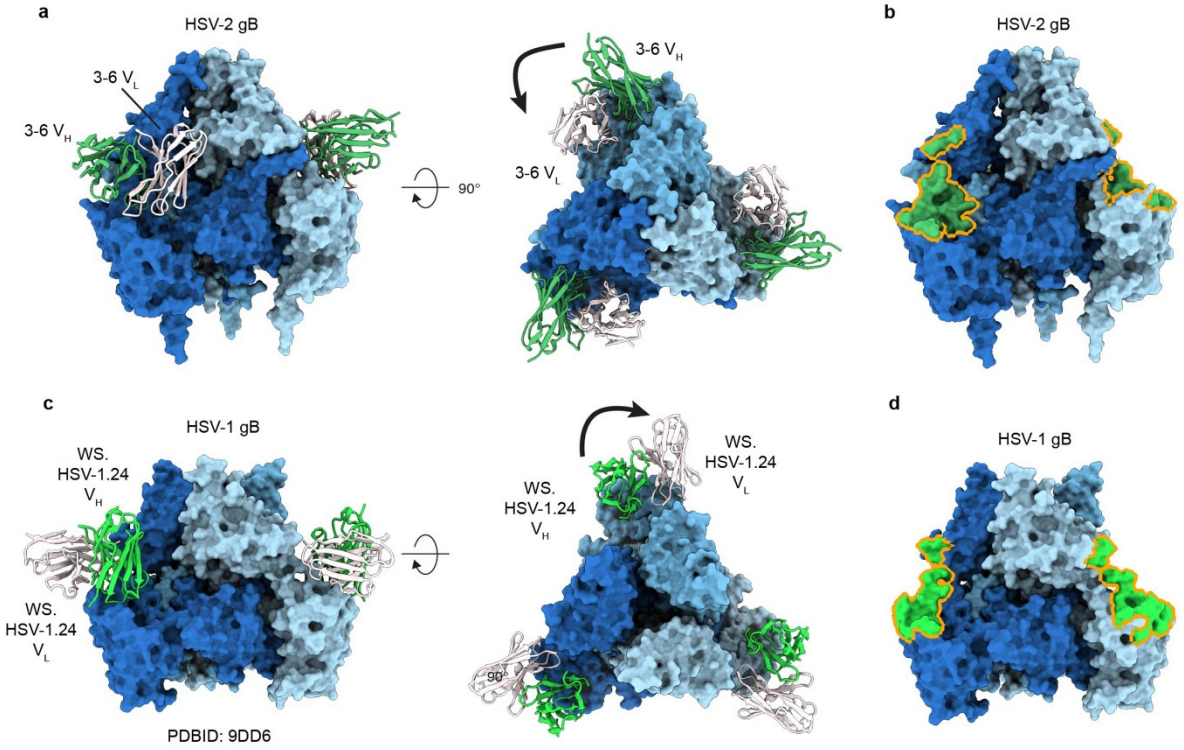

Extended Data Figure 13. Structural comparison of prefusion-specific Fab 3-6 and murine mAb WS.HSV-1.24. a, Side (*left*) and bottom (*right*) views of prefusion HSV-2 gB with three bound Fab 3-6. The 3-6 V_H is colored green, the V_L is colored white, and gB protomers are colored shades of blue. **b**, Side view showing the epitope footprint of Fab 3-6 on prefusion HSV-2 gB. Footprints are outlined in orange. **c**, Side (*left*) and bottom (*right*) views of prefusion HSV-1 gB with three bound Fab WS.HSV-1.24 (PDB ID: 9DD6). The WS.HSV-1.24 V_H is colored light green, the V_L is colored white, and gB protomers are colored shades of blue. **d**, Side view showing the epitope footprint of Fab WS.HSV-1.24 on prefusion HSV-1 gB.

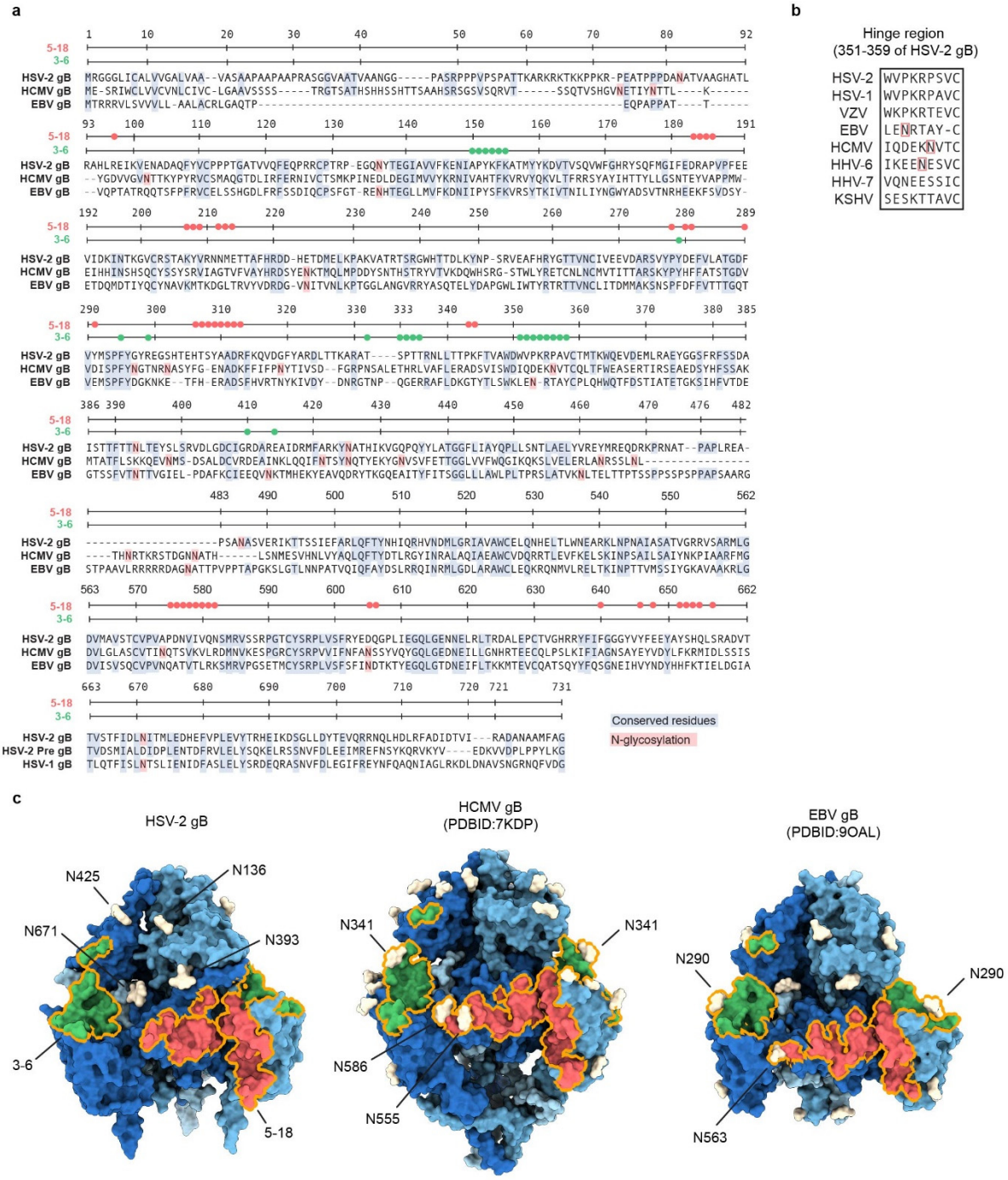

Extended Data Figure 14. Conservation and glycan shielding of HSV-2 prefusion-specific epitopes across human herpesvirus gBs. **a**, Sequence alignment of HSV-2 gB residues 1–731 (strain HG52), HCMV gB residues 1–711 (strain Towne), and EBV gB residues 1–692 (strain M81). Residues in the prefusion-specific epitopes of mAbs 5-18 (red) and 3-6 (green) are indicated above the alignments by colored circles. Conserved residues among HSV-2, HCMV,

and EBV gB are highlighted in blue, and *N*-linked glycosylation sites are shown in red. **b**, Sequence alignment of the domain (D)I–DII hinge-region residues from human herpesvirus gBs, with *N*-linked glycosylation sites in the hinge regions indicated by red boxes. **c**, Structural comparison of the glycan shield near prefusion-specific epitopes in HSV-2, HCMV, and EBV gB. HSV-2 gB glycans are modeled based on the HSV-2 gB–Fab 3-5 and 3-6 complex structure. HCMV gB (PDB ID: 7KDP) and EBV gB (PDB ID: 9OAL) *N*-linked glycans are modeled using the GlycoShape server[48]. The Fab 5-18 footprint is shown in red, the Fab 3-6 footprint in green, and both footprints are outlined in orange. Glycans are colored white. All built glycans are labeled for HSV-2, while only shielding glycans are labeled for HCMV and EBV gB.

Autoreactivity Summary Table – Intracellular and Extracellular IgG Binding (%)

mAb	HEp-2		HEK293-T	
	Intracellular (%)	Extracellular (%)	Intracellular (%)	Extracellular (%)
3-5	0.1	0.0	0.3	0.0
3-6	0.0	0.0	0.0	0.0
1-14	**6.6**	0.0	**17.2**	0.0
5-18	1.3	0.1	**5.3**	0.1
4E10 (+)	**97.8**	0.0	**100.0**	0.0
2F5 (+)	**7.1**	0.4	**20.4**	0.4
17B (-)	0.0	0.0	0.0	0.0
VRC01 (-)	**22.1**	0.0	**32.9**	0.0
2' only	0.0	0.0	0.0	0.0

Extended Data Table 1. Summary table of flow cytometry assay for intracellular and extracellular self-antigen recognition by prefusion-specific mAbs. Shown is the percent of antibody-bound HEp-2 and HEK293T live cell lines stained with mAbs intracellularly and extracellularly and gated for IgG-positive cells. Positive cutoff for autoreactivity set at 5% (bold).

Fab 5-18

HSV-2 gB : Fab 5-18 V_H

Protomer A

Hydrogen bonds

	Protomer A	Atom	Dist. [Å]	5-18 V_H	Atom	Position
1	ASN 212	[OD1]	3.11	SER 28	[OG]	HCDR1
2	ASP 183	[OD1]	3.14	ARG 32	[NH1]	HCDR1
3	ASP 183	[OD2]	2.96	ARG 32	[NH2]	HCDR1
4	ARG 184	[O]	3.85	ARG 32	[NH1]	HCDR1
5	LYS 207	[O]	3.52	ARG 32	[NH2]	HCDR1
5	ARG 313	[NH2]	3.85	ARG 32	[O]	HCDR1
6	ARG 313	[NH1]	2.87	TYR 35	[OH]	HCDR1
7	ARG 313	[NH2]	3.18	TYR 52	[OH]	HCDR2
8	GLU 214	[OE2]	3.35	TYR 53	[OH]	HCDR2
9	ASP 312	[OD2]	2.70	TYR 58	[OH]	HCDR2
11	TYR 291	[OH]	2.85	THR 100	[O]	HCDR3

Salt bridges

	Protomer A	Atom	Dist. [Å]	5-18 V_H	Atom	Position
1	ASP 183	[OD1]	3.88	ARG 32	[NH2]	HCDR1
2	ASP 183	[OD1]	3.14	ARG 32	[NH1]	HCDR1
3	ASP 183	[OD2]	2.96	ARG 32	[NH2]	HCDR1
4	ASP 183	[OD2]	3.57	ARG 32	[NH1]	HCDR1

Protomer C

Hydrogen bonds

	Protomer C	Atom	Dist. [Å]	5-18 V_H	Atom	Position
1	SER 653	[OH]	2.62	THR 100	[OG1]	HCDR3

HSV-2 gB : Fab 5-18 V_L

Protomer A

Hydrogen bonds

	Protomer A	Atom	Dist. [Å]	5-18 V_L	Atom	Position
1	ASP 280	[OD2]	2.8	SER 30	[OG]	LCDR1
2	SER 308	[O]	3.1	SER 93	[N]	LCDR3
3	SER 308	[O]	2.82	SER 93	[OG]	LCDR3

Protomer C

Hydrogen bonds

	Protomer C	Atom	Dist. [Å]	5-18 V_L	Atom	Position
1	SER 653	[O]	2.63	TYR 49	[OH]	LCDR2
2	GLN 655	[N]	2.99	SER 53	[OG]	LCDR2
3	GLN 655	[O]	3.38	SER 53	[OG]	LCDR2
4	TYR 652	[OH]	2.74	LEU 54	[O]	LCDR2
5	TYR 652	[OE1]	3.72	LEU 54	[N]	LCDR2
6	ASN 582	[OD1]	3.34	SER 56	[OG]	LCDR2
7	VAL 580	[O]	3.83	GLY 57	[N]	LCDR2
8	ASP576	[O]	3.72	SER 60	[OG]	LCDR2
9	ASP 576	[O]	3.41	ARG 61	[N]	LCDR2

Fab 1-14

HSV-2 gB : Fab 1-14 V_H

Protomer A

Hydrogen bonds

	Protomer A	Atom	Dist. [Å]	1-14 V_H	Atom	Position
1	PRO 343	[O]	3.9	TYR 52A	[OH]	HCDR2
2	GLU 214	[OE1]	3.27	HIS 55	[NE2]	HCDR2
3	ALA 311	[N]	3.03	ASP 58	[OD2]	HCDR2
4	ASN 212	[ND2]	2.85	SER 74	[OG]	H-FR3
5	TYR 291	[OH]	2.84	ARG 97	[NH2]	HCDR3
6	SER 308	[O]	3.12	GLU 100A	[N]	HCDR3
7	ALA 310	[N]	2.88	GLU 100A	[OE2]	HCDR3
8	ARG 313	[NH1]	3.15	GLU 100A	[OE1]	HCDR3
9	ARG 313	[NH1]	3.13	GLU 100A	[OE2]	HCDR3
10	THR 307	[O]	2.99	ASN 100B	[ND2]	HCDR3
11	SER 308	[O]	2.98	ASN 100B	[ND2]	HCDR3

Salt bridges

	Protomer A	Atom	Dist. [Å]	1-14 V_H	Atom	Position
1	GLU 214	[OE1]	3.27	HIS 55	[NE2]	HCDR2
2	ARG 313	[NH1]	3.15	GLU 100A	[OE1]	HCDR3
3	ARG 313	[NH1]	3.13	GLU 100A	[OE2]	HCDR3

Protomer C

Hydrogen bonds

	Protomer C	Atom	Dist. [Å]	1-14 V_H	Atom	Position
1	SER 653	[OG]	3.8	ARG 97	[NH2]	HCDR3
2	TYR 652	[O]	3.76	GLN 98	[NE2]	HCDR3

HSV-2 gB : Fab 1-14 V_L

Protomer A

Hydrogen bonds

	Protomer A	Atom	Dist. [Å]	1-14 V_L	Atom	Position
1	ASP 280	[OD2]	2.89	SER 30	[OG]	LCDR1
2	THR 307	[N]	3.08	HIS 92	[O]	LCDR3
3	TYR 309	[O]	2.85	TRP 94	[NE1]	LCDR3

Extended Data Table 2. Interface analysis of mAbs 5-18 and 1-14 with prefusion-stabilized HSV-2 gB (PDBePISA).

Fab 3-6

HSV-2 gB : Fab 3-6 V_H

Hydrogen bonds

	Protomer A	Atom	Dist. [Å]	3-6 V_H	Atom	Position
1	GLU 414	[OE1]	3.53	GLN 1	[N]	H-FR1
2	ALA 357	[O]	2.98	ASN 28	[ND2]	H-FR1
3	VAL 358	[O]	3.84	ASN 28	[ND2]	H-FR1
4	ARG 355	[NE]	2.86	SER 31	[O]	HCDR1
5	ARG 355	[NH2]	2.87	SER 31	[O]	HCDR1
6	PRO 356	[O]	2.71	SER 31	[OG]	HCDR1
7	PRO 353	[O]	2.84	TYR 52A	[OH]	HCDR2
8	PRO 334	[O]	2.97	ARG 56	[NH1]	HCDR2
9	LYS 153	[N]	3.46	TRP 100	[O]	HCDR3
10	LYS 153	[O]	2.82	SER 100A	[OG]	HCDR3
11	LYS 153	[O]	2.85	GLY 100B	[N]	HCDR3
12	TYR 336	[N]	3.21	GLY 100C	[N]	HCDR3
13	THR 336	[N]	3.21	TYR 100 G	[OH]	HCDR3
14	TRP 351	[O]	2.92	TYR 100 G	[OH]	HCDR3
15	ARG 299	[NH1]	3.75	TYR 100 F	[OH]	HCDR3

Salt bridges

	Protomer A	Atom	Dist. [Å]	3-6 V_H	Atom	Position
1	GLU 414	[OE1]	3.53	GLN 1	[N]	H-FR1

HSV-2 gB : Fab 3-6 V_L

Hydrogen bonds

	Protomer A	Atom	Dist. [Å]	3-6 V_H	Atom	Position
1	SER 333	[OG]	3.65	ASP 93	[O]	LCDR3

Fab 3-5

HSV-2 gB : Fab 3-5 V_H

Hydrogen bonds

	Protomer A	Atom	Dist. [Å]	3-5 V_H	Atom	Position
1	VAL 168	[O]	3.86	SER 30	[O]	HCDR1
2	MET 178	[SD]	3.75	SER 30	[OG]	HCDR1
3	ARG 210	[O]	2.8	TYR 32	[OH]	HCDR1
4	ASN 211	[O]	3.81	TYR 32	[OH]	HCDR1
5	THR 216	[O]	3.79	TYR 33	[OH]	HCDR1
6	VAL 168	[N]	3.63	PRO 53	[O]	HCDR2
7	PHE 170	[N]	3.01	THR 73	[OG1]	H-FR3
8	PHE 170	[O]	3.16	THR 73	[N]	H-FR3
9	PHE 170	[O]	2.86	THR 73	[OG1]	H-FR3
10	PHE 170	[O]	3.7	SER 74	[N]	H-FR3
11	GLU 214	[O]	3.25	ARG 94	[NH1]	HCDR3
12	GLU 214	[O]	2.91	ARG 94	[NH2]	HCDR3
13	THR 215	[OG1]	2.87	ARG 94	[NH2]	HCDR3
14	THR 216	[N]	2.99	SER 96	[O]	HCDR3
15	GLU 214	[O]	3.66	TYR 99	[OH]	HCDR3
16	GLU 214	[OE2]	3.19	TYR 102	[OH]	HCDR3

HSV-2 gB : Fab 3-5 V_L

Hydrogen bonds

	Protomer A	Atom	Dist. [Å]	3-5 V_L	Atom	Position
1	GLU 224	[O]	2.82	TYR 30	[OH]	LCDR1
2	ARG 203	[NH2]	3.24	ASN 31	[OD1]	LCDR1
3	THR 205	[OG1]	2.96	TYR 32	[OH]	LCDR1
4	GLU 224	[OE2]	2.74	TYR 32	[OH]	LCDR1
5	ASP 221	[O]	3.12	ARG 95B	[NH1]	LCDR3
6	ASP 221	[O]	2.82	ARG 95B	[NH2]	LCDR3
7	ASP 222	[OD1]	3.78	ARG 95B	[NH2]	LCDR3

Salt bridges

	Protomer A	Atom	Dist. [Å]	3-5 V_L	Atom	Position
1	ASP 222	[OD1]	3.78	ARG 95B	[NH2]	LCDR3

Extended Data Table 3. Interface analysis of mAbs 3-6 and 3-5 with prefusion-stabilized HSV-2 gB (PDBePISA).

Sample	gB-G3 (prefusion HSV-2 gB) + 5-18 Fab	gB-G3 (prefusion HSV-2 gB) + 1-14 Fab	gB-G3 (prefusion HSV-2 gB) + 3-6 and 3-5 Fabs
PDB ID	10UD	11AB	11BH
EMDB code	EMD-75469	EMD-75581	EMD-75602
Cryo-EM data collection			
Microscope	FEI Glacios	FEI Glacios	FEI Glacios
Voltage (kV)	200	200	200
Detector	Falcon 4	Falcon 4	Falcon 4
Magnification (nominal)	150,000	150,000	150,000
Pixel size (Å/pix)	0.933	0.933	0.933
Exposure dose ($e^-/Å^2$)	49	49	49
Defocus range (μm)	1.5 – 2.5	1.5 – 2.5	0.0 – 1.0
Tilt angle (°)	30	30	0
Micrographs collected	2,551	2,553	3,060
Micrographs used	1,780	2,413	2,244
Particles extracted	672,460	717,716	465,098
Automation software	SerialEM	SerialEM	SerialEM
3D reconstruction statistics			
Particles	201,551	330,805	37,512
Symmetry	C3	C3	C3
Map sharpening B-factor	128.1	160.3	91.0
Unmasked: 0.5	3.8	3.8	4.3
Masked: 0.5	3.2	3.5	3.6
Unmasked: 0.143	3.4	3.6	3.7
Masked: 0.143	2.9	3.2	3.1
Model refinement and validation statistics			
Sharpening tool	EMReady v2.2.2	EMReady v2.2.2	EMReady v2.2.2
Refinement package	PHENIX	PHENIX	PHENIX
Composition			
Non-hydrogen atoms	19,824	19,656	25,491
Amino Acids	2,487	2,466	3,225
Ligands (type)	6 (6 NAG)	3 (3 NAG)	15 (3 BMA, 12 NAG)
Bonds (RMSD)			
Length (Å)	0.005	0.004	0.004
Angles (°)	0.97	0.947	0.948
Ramachandran plot			
Favored (%)	97.52	97.45	97.65
Allowed (%)	2.48	2.55	2.35
Outliers (%)	0.0	0.0	0.0
Rotamer outliers (%)	0.0	0.09	0.11
Cβ outliers (%)	0.0	0.0	0.0
CaBLAM outliers (%)	1.03	2.34	1.36
ADP (B-factors)			
Amino Acids (mean)	42.1	75.0	69.8
Ligands (mean)	101.6	97.1	130.3
CC (mask)	0.89	0.89	0.89
MolProbity score	1.15	1.20	1.06
Clash score	2.61	3.03	2.08
Overall mean Q-Score	0.67	0.60	0.58

Extended Data Table 4. Cryo-EM Data collection and refinement statistics.

REFERENCES

1 De Rose, D. U. *et al.* Neonatal herpes simplex virus infection: From the maternal infection to the child outcome. *Journal of Medical Virology* **95** (2023). https://doi.org:10.1002/jmv.29024

2 Arduino, P. G. & Porter, S. R. Herpes Simplex Virus Type 1 infection: overview on relevant clinico-pathological features*. *Journal of Oral Pathology & Medicine* **37**, 107-121 (2008). https://doi.org:10.1111/j.1600-0714.2007.00586.x

3 Muller, W. J. Treatment of perinatal viral infections to improve neurologic outcomes. *Pediatric Research* **81**, 162-169 (2017). https://doi.org:10.1038/pr.2016.191

4 Jones, C. A., Walker, K. S. & Badawi, N. Antiviral agents for treatment of herpes simplex virus infection in neonates. *Cochrane Database of Systematic Reviews* **2010** (2009). https://doi.org:10.1002/14651858.cd004206.pub2

5 Connolly, S. A., Jardetzky, T. S. & Longnecker, R. The structural basis of herpesvirus entry. *Nature Reviews Microbiology* **19**, 110-121 (2021). https://doi.org:10.1038/s41579-020-00448-w

6 McLellan, J. S. *et al.* Structure of RSV Fusion Glycoprotein Trimer Bound to a Prefusion-Specific Neutralizing Antibody. *Science* **340**, 1113-1117 (2013). https://doi.org:doi:10.1126/science.1234914

7 Ngwuta, J. O. *et al.* Prefusion F–specific antibodies determine the magnitude of RSV neutralizing activity in human sera. *Science Translational Medicine* **7**, 309ra162-309ra301 (2015). https://doi.org:10.1126/scitranslmed.aac4241

8 Sanders, R. W. *et al.* HIV-1 neutralizing antibodies induced by native-like envelope trimers. *Science* **349**, aac4223-aac4223 (2015). https://doi.org:10.1126/science.aac4223

9 Rossey, I., McLellan, J. S., Saelens, X. & Schepens, B. Clinical Potential of Prefusion RSV F-specific Antibodies. *Trends in Microbiology* **26**, 209-219 (2018). https://doi.org:10.1016/j.tim.2017.09.009

10 Callaway, H. M. *et al.* Structure of the rabies virus glycoprotein trimer bound to a prefusion-specific neutralizing antibody. *Science Advances* **8**, eabp9151 (2022). https://doi.org:doi:10.1126/sciadv.abp9151

11 Vollmer, B. *et al.* A nanobody specific to prefusion glycoprotein B neutralizes HSV-1 and HSV-2. *Nature* (2025). https://doi.org:10.1038/s41586-025-09438-5

12 Roark, R. S. *et al.* Prefusion structure, evasion and neutralization of HSV-1 glycoprotein B. *Nature Microbiology* **10**, 2966-2980 (2025). https://doi.org:10.1038/s41564-025-02153-x

13 Setliff, I. *et al.* High-Throughput Mapping of B Cell Receptor Sequences to Antigen Specificity. *Cell* **179**, 1636-1646.e1615 (2019). https://doi.org:10.1016/j.cell.2019.11.003

14 Connolly, S. A., Jackson, J. O., Jardetzky, T. S. & Longnecker, R. Fusing structure and function: a structural view of the herpesvirus entry machinery. *Nature Reviews Microbiology* **9**, 369-381 (2011). https://doi.org:10.1038/nrmicro2548

15 James, C. *et al.* Herpes simplex virus: global infection prevalence and incidence estimates, 2016. *Bulletin of the World Health Organization* **98**, 315-329 (2020). https://doi.org:10.2471/blt.19.237149

16 Engman, M.-L. *et al.* Neuropsychologic Outcomes in Children With Neonatal Herpes Encephalitis. *Pediatric Neurology* **38**, 398-405 (2008). https://doi.org:10.1016/j.pediatrneurol.2008.02.005

17 Brown, Z. A. *et al.* Effect of Serologic Status and Cesarean Delivery on Transmission Rates of Herpes Simplex Virus From Mother to Infant. *JAMA* **289**, 203 (2003). https://doi.org:10.1001/jama.289.2.203
18 Kimberlin, D. W. *et al.* Oral Acyclovir Suppression and Neurodevelopment after Neonatal Herpes. *New England Journal of Medicine* **365**, 1284-1292 (2011). https://doi.org:10.1056/nejmoa1003509
19 Kimberlin, D. W. *et al.* The Safety and Efficacy of High-Dose (HD) Acyclovir (ACV) in Neonatal Herpes Simplex Virus (HSV) Infections. *Pediatric Research* **45**, 165A-165A (1999). https://doi.org:10.1203/00006450-199904020-00980
20 Whitley, R., Davis, E. A. & Suppapanya, N. Incidence of Neonatal Herpes Simplex Virus Infections in a Managed-Care Population. *Sexually Transmitted Diseases* **34**, 704-708 (2007). https://doi.org:10.1097/01.olq.0000258432.33412.e2
21 Heldwein, E. E. & Krummenacher, C. Entry of herpesviruses into mammalian cells. *Cellular and Molecular Life Sciences* **65**, 1653-1668 (2008). https://doi.org:10.1007/s00018-008-7570-z
22 Cooper, R. S., Georgieva, E. R., Borbat, P. P., Freed, J. H. & Heldwein, E. E. Structural basis for membrane anchoring and fusion regulation of the herpes simplex virus fusogen gB. *Nature Structural & Molecular Biology* **25**, 416-424 (2018). https://doi.org:10.1038/s41594-018-0060-6
23 Harrison, S. C. Viral membrane fusion. *Virology* **479-480**, 498-507 (2015). https://doi.org:10.1016/j.virol.2015.03.043
24 Nicola, A. V. Herpesvirus Entry into Host Cells Mediated by Endosomal Low <scp>pH</scp>. *Traffic* **17**, 965-975 (2016). https://doi.org:10.1111/tra.12408
25 Sathiyamoorthy, K., Chen, J., Longnecker, R. & Jardetzky, T. S. The COMPLEXity in herpesvirus entry. *Current Opinion in Virology* **24**, 97-104 (2017). https://doi.org:10.1016/j.coviro.2017.04.006
26 Backovic, M. & Jardetzky, T. S. Class III viral membrane fusion proteins. *Current Opinion in Structural Biology* **19**, 189-196 (2009). https://doi.org:10.1016/j.sbi.2009.02.012
27 Atanasiu, D., Saw, W. T., Cohen, G. H. & Eisenberg, R. J. Cascade of Events Governing Cell-Cell Fusion Induced by Herpes Simplex Virus Glycoproteins gD, gH/gL, and gB. *Journal of Virology* **84**, 12292-12299 (2010). https://doi.org:10.1128/jvi.01700-10
28 McLellan, J. S. Neutralizing epitopes on the respiratory syncytial virus fusion glycoprotein. *Current Opinion in Virology* **11**, 70-75 (2015). https://doi.org:10.1016/j.coviro.2015.03.002
29 McLellan, J. S. *et al.* Structure-Based Design of a Fusion Glycoprotein Vaccine for Respiratory Syncytial Virus. *Science* **342**, 592-598 (2013). https://doi.org:doi:10.1126/science.1243283
30 Zhong, L. *et al.* Targeting herpesvirus entry complex and fusogen glycoproteins with prophylactic and therapeutic agents. *Trends in Microbiology* **31**, 788-804 (2023). https://doi.org:10.1016/j.tim.2023.03.001
31 Backes, I. M., Leib, D. A. & Ackerman, M. E. Monoclonal antibody therapy of herpes simplex virus: An opportunity to decrease congenital and perinatal infections. *Frontiers in Immunology* **13** (2022). https://doi.org:10.3389/fimmu.2022.959603

32 Slein, M. D. *et al.* Effector functions are required for broad and potent protection of neonatal mice with antibodies targeting HSV glycoprotein D. *Cell Reports Medicine* **5**, 101417 (2024). https://doi.org:10.1016/j.xcrm.2024.101417
33 Slein, M. D. *et al. Antibodies targeting HSV glycoprotein B require effector functions to protect neonatal mice* (Cold Spring Harbor Laboratory, 2025).
34 Wang, K. *et al.* Monoclonal Antibodies, Derived from Humans Vaccinated with the RV144 HIV Vaccine Containing the HVEM Binding Domain of Herpes Simplex Virus (HSV) Glycoprotein D, Neutralize HSV Infection, Mediate Antibody-Dependent Cellular Cytotoxicity, and Protect Mice. *Journal of Virology* **91**, e00411-00417 (2017). https://doi.org:10.1128/jvi.00411-17
35 Seyfizadeh, N. *et al.* Development of a highly effective combination monoclonal antibody therapy against Herpes simplex virus. *Journal of Biomedical Science* **31** (2024). https://doi.org:10.1186/s12929-024-01045-2
36 Kuraoka, M. *et al.* A non-neutralizing glycoprotein B monoclonal antibody protects against herpes simplex virus disease in mice. *Journal of Clinical Investigation* **133** (2023). https://doi.org:10.1172/jci161968
37 Bender, F. C. *et al.* Antigenic and Mutational Analyses of Herpes Simplex Virus Glycoprotein B Reveal Four Functional Regions. *Journal of Virology* **81**, 3827-3841 (2007). https://doi.org:10.1128/jvi.02710-06
38 Sun, C. *et al.* The structure of HSV-1 gB bound to a potent neutralizing antibody reveals a conservative antigenic domain across herpesviruses. *hLife* **2**, 141-146 (2024). https://doi.org:https://doi.org/10.1016/j.hlife.2023.12.004
39 Pötzsch, S. *et al.* B Cell Repertoire Analysis Identifies New Antigenic Domains on Glycoprotein B of Human Cytomegalovirus which Are Target of Neutralizing Antibodies. *PLOS Pathogens* **7**, e1002172 (2011). https://doi.org:10.1371/journal.ppat.1002172
40 Stellbrink, H.-J. *et al.* Safety and efficacy of monoclonal antibody therapy in patients with chronic herpes simplex virus-2 genital infections: MATCH-2, a randomized double-blinded, parallel-group phase 2 multi-center trial. *Pharmacological Research* **221**, 107999 (2025). https://doi.org:10.1016/j.phrs.2025.107999
41 Krawczyk, A. *et al.* Overcoming drug-resistant herpes simplex virus (HSV) infection by a humanized antibody. *Proceedings of the National Academy of Sciences* **110**, 6760-6765 (2013). https://doi.org:10.1073/pnas.1220019110
42 Sponholtz, M. R. *et al. Structure-based design of soluble prefusion-stabilized herpes simplex virus type 2 glycoprotein B antigens* (openRxiv, 2026).
43 Sponholtz, M. R. *et al.* Structure-based design of a soluble human cytomegalovirus glycoprotein B antigen stabilized in a prefusion-like conformation. *Proceedings of the National Academy of Sciences* **121** (2024). https://doi.org:10.1073/pnas.2404250121
44 McCool, R. S. *et al.* Structure and immunogenicity of an engineered soluble prefusion-stabilized EBV gB antigen. *Nature Communications* (2026). https://doi.org:10.1038/s41467-025-67969-x
45 Mori H, N. T., Shimizu H, Koube A. NTI-HSV gb monoclonal antibody or antigen-binding fragment thereof. (2020).
46 Liu, Y. *et al.* Prefusion structure of human cytomegalovirus glycoprotein B and structural basis for membrane fusion. *Science Advances* **7**, eabf3178 (2021). https://doi.org:doi:10.1126/sciadv.abf3178

47 McCool, R. S. *et al.* Structure and immunogenicity of an engineered soluble prefusion-stabilized EBV gB antigen. *Nat Commun* **17**, 1197 (2026). https://doi.org:10.1038/s41467-025-67969-x
48 Ives, C. M. *et al.* Restoring protein glycosylation with GlycoShape. *Nature Methods* **21**, 2117-2127 (2024). https://doi.org:10.1038/s41592-024-02464-7
49 Szucs, T. D., Berger, K., Fisman, D. N. & Harbarth, S. The estimated economic burden of genital herpes in the United States. An analysis using two costing approaches. *BMC Infectious Diseases* **1** (2001). https://doi.org:10.1186/1471-2334-1-5
50 Silva, S., Ayoub, H. H., Johnston, C., Atun, R. & Abu-Raddad, L. J. Estimated economic burden of genital herpes and HIV attributable to herpes simplex virus type 2 infections in 90 low- and middle-income countries: A modeling study. *PLOS Medicine* **19**, e1003938 (2022). https://doi.org:10.1371/journal.pmed.1003938
51 Madavaraju, K., Koganti, R., Volety, I., Yadavalli, T. & Shukla, D. Herpes Simplex Virus Cell Entry Mechanisms: An Update. *Frontiers in Cellular and Infection Microbiology* **10** (2021). https://doi.org:10.3389/fcimb.2020.617578
52 Johnson, D. C., Wisner, T. W. & Wright, C. C. Herpes Simplex Virus Glycoproteins gB and gD Function in a Redundant Fashion To Promote Secondary Envelopment. *Journal of Virology* **85**, 4910-4926 (2011). https://doi.org:10.1128/jvi.00011-11
53 Milojević, L. *et al.* Capturing intermediates and membrane remodeling in class III viral fusion. *Science Advances* **10** (2024). https://doi.org:10.1126/sciadv.adn8579
54 Kim, M., Qiao, Z., Yu, J., Montefiori, D. & Reinherz, E. L. Immunogenicity of recombinant human immunodeficiency virus type 1-like particles expressing gp41 derivatives in a pre-fusion state. *Vaccine* **25**, 5102-5114 (2007). https://doi.org:10.1016/j.vaccine.2006.09.071
55 Kulp, D. W. *et al.* Structure-based design of native-like HIV-1 envelope trimers to silence non-neutralizing epitopes and eliminate CD4 binding. *Nature Communications* **8**, 1655 (2017). https://doi.org:10.1038/s41467-017-01549-6
56 Kimberlin, D. W. *et al.* Safety and Efficacy of High-Dose Intravenous Acyclovir in the Management of Neonatal Herpes Simplex Virus Infections. *Pediatrics* **108**, 230-238 (2001). https://doi.org:10.1542/peds.108.2.230
57 Friedman, H. M. *et al.* Immune evasion properties of herpes simplex virus type 1 glycoprotein gC. *Journal of Virology* **70**, 4253-4260 (1996). https://doi.org:10.1128/jvi.70.7.4253-4260.1996
58 Akhtar, L. N. *et al.* Genotypic and Phenotypic Diversity of Herpes Simplex Virus 2 within the Infected Neonatal Population. *mSphere* **4** (2019). https://doi.org:10.1128/msphere.00590-18
59 Manivanh, R., Mehrbach, J., Knipe, D. M. & Leib, D. A. Role of Herpes Simplex Virus 1 γ34.5 in the Regulation of IRF3 Signaling. *Journal of Virology* **91** (2017). https://doi.org:10.1128/jvi.01156-17
60 Rader, K. A., Ackland-Berglund, C. E., Miller, J. K., Pepose, J. S. & Leib, D. A. In vivo characterization of site-directed mutations in the promoter of the herpes simplex virus type 1 latency-associated transcripts. *Journal of General Virology* **74**, 1859-1869 (1993). https://doi.org:10.1099/0022-1317-74-9-1859
61 Sponholtz, M. R. *et al.* Structure-based design of soluble prefusion-stabilized herpes simplex virus type 2 glycoprotein B antigens. *bioRxiv*, 2026.2001.2026.701809 (2026). https://doi.org:10.64898/2026.01.26.701809

62 Abu-Shmais, A. A. *et al.* Antibody sequence determinants of viral antigen specificity. *mBio* **15** (2024). https://doi.org:10.1128/mbio.01560-24
63 Alamyar, E., Giudicelli, V., Duroux, P. & Lefranc, M.-P. in *Journées Ouvertes de Biologie, Informatique et Mathématiques* 60 (Montpellier, France, 2010).
64 Wasdin, P. T. *et al.* Generation of antigen-specific paired-chain antibodies using large language models. *Cell* **188**, 7206-7221.e7216 (2025). https://doi.org:10.1016/j.cell.2025.10.006
65 Abanades, B. *et al.* The Patent and Literature Antibody Database (PLAbDab): an evolving reference set of functionally diverse, literature-annotated antibody sequences and structures. *Nucleic Acids Research* **52**, D545-D551 (2024). https://doi.org:10.1093/nar/gkad1056
66 Lefranc, M. P. *et al.* IMGT(R), the international ImMunoGeneTics information system(R). *Nucleic Acids Research* **37**, D1006-D1012 (2009). https://doi.org:10.1093/nar/gkn838
67 Raybould, M. I. J., Kovaltsuk, A., Marks, C. & Deane, C. M. CoV-AbDab: the coronavirus antibody database. *Bioinformatics* **37**, 734-735 (2021). https://doi.org:10.1093/bioinformatics/btaa739
68 Yoon, H. *et al.* CATNAP: a tool to compile, analyze and tally neutralizing antibody panels. *Nucleic Acids Research* **43**, W213-W219 (2015). https://doi.org:10.1093/nar/gkv404
69 Kovaltsuk, A. *et al.* Observed Antibody Space: A Resource for Data Mining Next-Generation Sequencing of Antibody Repertoires. *The Journal of Immunology* **201**, 2502-2509 (2018). https://doi.org:10.4049/jimmunol.1800708
70 Raybould, M. I. J. *et al.* Thera-SAbDab: the Therapeutic Structural Antibody Database. *Nucleic Acids Research* **48**, D383-D388 (2020). https://doi.org:10.1093/nar/gkz827
71 Dudzic, P. *et al.* Conserved heavy/light contacts and germline preferences revealed by a large-scale analysis of natively paired human antibody sequences and structural data. *Communications Biology* **8** (2025). https://doi.org:10.1038/s42003-025-08388-y
72 Bateman, A. *et al.* UniProt: the Universal Protein Knowledgebase in 2023. *Nucleic Acids Research* **51**, D523-D531 (2023). https://doi.org:10.1093/nar/gkac1052
73 Mastronarde, D. N. Automated electron microscope tomography using robust prediction of specimen movements. *Journal of Structural Biology* **152**, 36-51 (2005). https://doi.org:https://doi.org/10.1016/j.jsb.2005.07.007
74 Punjani, A., Rubinstein, J. L., Fleet, D. J. & Brubaker, M. A. cryoSPARC: algorithms for rapid unsupervised cryo-EM structure determination. *Nature Methods* **14**, 290-296 (2017). https://doi.org:10.1038/nmeth.4169
75 Cao, H., Li, T., He, J. & Huang, S. BPS2025 - EMReady2: A general model for improving cryo-EM and cryo-ET maps by heterogeneity-aware deep learning. *Biophysical Journal* **124**, 625a (2025). https://doi.org:10.1016/j.bpj.2024.11.3223
76 Morin, A. *et al.* Collaboration gets the most out of software. *eLife* **2**, e01456 (2013). https://doi.org:10.7554/eLife.01456
77 Abramson, J. *et al.* Accurate structure prediction of biomolecular interactions with AlphaFold 3. *Nature* **630**, 493-500 (2024). https://doi.org:10.1038/s41586-024-07487-w
78 Pettersen, E. F. *et al.* <scp>UCSF ChimeraX</scp>: Structure visualization for researchers, educators, and developers. *Protein Science* **30**, 70-82 (2021). https://doi.org:10.1002/pro.3943

79 Emsley, P. & Cowtan, K. Coot: model-building tools for molecular graphics. *Acta Crystallographica Section D Biological Crystallography* **60**, 2126-2132 (2004). https://doi.org:10.1107/s0907444904019158

80 Liebschner, D. *et al.* Macromolecular structure determination using X-rays, neutrons and electrons: recent developments in Phenix. *Acta Crystallographica Section D Structural Biology* **75**, 861-877 (2019). https://doi.org:10.1107/s2059798319011471

81 Croll, T. I. ISOLDE: a physically realistic environment for model building into low-resolution electron-density maps. *Acta Crystallographica Section D Structural Biology* **74**, 519-530 (2018). https://doi.org:10.1107/s2059798318002425

82 Sievers, F. & Higgins, D. G. Clustal Omega for making accurate alignments of many protein sequences. *Protein Science* **27**, 135-145 (2018). https://doi.org:10.1002/pro.3290